Numerical simulation of nonsmooth multibody systems with switching bilateral constraints

Indrajeet Patil* and Olivier Brüls
Department of Aerospace and Mechanical Engineering,
University of Liège, Belgium.

*Corresponding author: Indrajeet Patil (ikpatil@uliege.be)

Abstract

This paper addresses a special class of multibody systems where switching functions trigger instantaneous changes in the bilateral constraints, thus leading to a time-discontinuous response. These switching functions define switching surfaces, that partition the system dynamics into different domains with nonsmooth transitions. Switching surfaces are thus instrumental in the proposed modelling framework, as they orchestrate the geometry of the constraint space. The equations of motion can either be expressed as hybrid differential-algebraic equations or as an equality of differential measures with constraints. At switching, an impact law based on an intermediate gradient is introduced and we suggest to determine this intermediate gradient by interpolation between the pre- and post-switch gradients. Theoretical arguments and numerical results show that the choice of this intermediate gradient drives the energy behavior at switching. The numerical integration demands special attention, as classical DAE solvers fail to handle discontinuities at switching surfaces. Event-driven and time-stepping schemes from nonsmooth dynamics are well-suited for this class of problems. We use a benchmark test to compare the solutions obtained from classical and nonsmooth versions of the generalized-α method. Further, using the nonsmooth generalized-α method, three examples of multibody systems with switching bilateral constraints are successfully simulated.

Keywords: Nonsmooth dynamics, Switching bilateral constraints, Differential-algebraic equations, Switching dynamical systems, Generalized-α method.

1 Introduction

Multibody systems are defined as an assembly of mechanical components, that interact with each other through kinematic joints, contact conditions, and force elements [1]. Geometric constraints thus play a crucial role in their modelling, as they restrict the relative motion between the interconnected bodies. These motion constraints can be of bilateral or unilateral nature. Unilateral or one-sided constraints involve inequalities as they restrict motion in only one direction [2] and are thus used represent non-penetration conditions during contacts. In this case, the system switches between unconstrained and constrained states. For instance, the well-studied example of a bouncing ball involves instantaneous transitions from an unconstrained state (free flight) to a constrained state (contact with the ground). The system dynamics is thus governed by a conditional statements, that takes the form of a complementarity condition [3]. In addition, an impact model is essential to obtain the complete equations of motion. Such orchestration of the first principles of mechanics by switching conditions result in solution trajectories that are not smooth or differentiable everywhere. Thus the treatment of unilateral constraints have garnered substantial attention [4–6], due to their inherent complexities, and are a well-established topic of research.

However, it is often assumed that bilateral or two-sided constraints satisfy sufficient continuity and differentiability conditions. This does not necessarily hold, as conditional statements may also trigger abrupt changes in the algebraic constraint expressions. In such situations, the system maintains a constrained state throughout, but the instantaneous switch creates a nonsmooth response with jumps in state variables. The system dynamics is thus dictated by nonsmooth or non-differentiable bilateral constraints. Importantly, the equations of motion of such multibody systems can be expressed in the form of switched differential-algebraic equations (DAEs) [7, 8], which differ both from classical DAEs and from systems with unilateral constraints. As a result, the mathematical modelling and numerical integration require a specialized treatment. However, there is a scarcity of scientific research to address the problem of switching bilateral constraints in the field of multibody systems. This paper thus aims to extend the current knowledge, by presenting a general modelling procedure and possible numerical integration methods for multibody systems with switching bilateral constraints.

The problem of switched DAEs in multibody systems can be related with another class of problems pertaining to the field of switching dynamical systems [9–13]. Such problems are encountered in electronic circuits, control systems and optimal control [14], automation, variable structure systems (VSS), sliding mode control [15], etc. Essentially, the expression of the conditional statements can be based on the definition of switching surfaces [16], that punctuate the system dynamics into continuous (smooth) and discrete (impulsive) dynamical regimes or modes. Smooth modes form a continuum, and the switching function is constructed so as to separate them by switching surfaces. In switched systems, some continuous and discrete time dynamics coexist and interact with each other, as the solution evolves across the switching surfaces. The switching functions can be constructed either based on state variables, or exogeneous signals, or a combination of both. Some of these concepts will be exploited in this paper, and adapted to the treatment of switching bilateral constraints, and fundamental differences will also be highlighted.

In this paper, we will show that the nonsmooth equations of motion of multibody systems with switching bilateral constraints can be either developed as hybrid differential-algebraic equations (HDAEs), or formulated based on an equality of differential measures. The hybrid approach relies on explicit information of the interactions between continuous and discrete regimes [17–20]. In our case, the HDAE form comprises of two sets of equations: (i) a standard DAE that holds in the smooth modes, and (ii) an impact equation that defines the impulsive dynamics at the switching surfaces. Alternatively, the concept of differential measures [21,22] can be exploited to formulate a unified equation which holds both in the smooth modes and at the switching surfaces. In this work, we present the equations of motion in both forms, which both lend themselves to particular classes of numerical schemes.

Further, we also address the formulation of the impact model in the equations of motion. We highlight that the equations of motion suffer from an indeterminacy in the constraint reaction force at switching surfaces. This indeterminacy arises from the indeterminacy of the constraint gradient at switching surfaces. For instance, the reaction force may be assumed to be aligned along the direction of the pre-switch gradient, or along the post-switch gradient, or along an intermediate gradient. We propose to fix this indeterminacy using an interpolation parameter, which determines an intermediate constraint gradient at switching by interpolation between the pre- and post-switch gradients. Then, the impact model is based on this intermediate gradient. For systems with a single constraint, we show that a simple interpolation formula can be used for that purpose. Theoretical arguments and numerical results demonstrate that the interpolation parameter drives the behaviour of energy at the switching surface. Thus, the interpolation parameter is an important parameter of the model, which controls the system dynamics at the switching surfaces. For more complex cases involving multiple constraints, we show that standard interpolation formulae are not directly applicable and that more sophisticated approaches using subspace interpolation methods could be considered.

Special care is required for the numerical integration of switched DAEs [23,24]. Classical DAE solvers fail to deal with the discontinuities at velocity and acceleration levels which may occur at the switching events. Smooth approximations can be introduced in the model, but the trajectories may either deviate from the exact solution, or induce high numerical stiffness. Instead, numerical methods for nonsmooth dynamical systems can be considered [25]. Systems defined using hybrid models lend themselves to event-driven schemes. Event-driven algorithms combine classical DAE schemes, a switch-detection with a time-step adaptation, and an update procedure at each event. A benefit of these algorithms is that higher order DAE schemes can be used in the smooth phases of motion. However, event-driven schemes suffer from several drawbacks [26], such as when explicit information on switching cannot be obtained, and when the number of switches is high. Alternatively, formulations based on an equality of differential measures lend themselves to numerical integration using time-stepping schemes [27,28]. Such schemes accommodate for switching events within a time step and thus do not require special adaptations of the time step. However, these schemes are limited to first-order accuracy [29], as the impulsive contributions are not precisely localized within the time step.

In this paper, we will study the classical index-3, index-reduced, event-driven, and nonsmooth versions of the generalized-α method. A comparison of numerical results obtained using classical and nonsmooth solvers shall be presented for a benchmark test of a system with a single switching surface. This analysis will reveal that the nonsmooth generalized-α method (NSGA) [28] is an appropriate choice to handle such class of problems. Further using the NSGA method, we successfully simulate three additional multibody systems with switching bilateral constraints: a simplified braiding machine, a wheel rolling over a pothole, and a cam-follower mechanism.

The paper is structured as follows. In Section 2, the role of switching surfaces in the modelling procedure is demonstrated for a simple benchmark example. Detailed formulations are presented for a system with a single switching surface, and further generalized to systems with multiple surfaces. In Section 3, we develop the equations of motion both as hybrid differential-algebraic equations (HDAEs) and based on an equality of differential measures, along with the impact model. In Section 4, we present several possible numerical time integration schemes. Numerical examples are addressed in Section 5, and the paper is finally concluded in Section 6, with highlights on future perspectives.

2 Bilateral constraints and switching surfaces

Consider a multibody system whose dynamics evolves with a number $m^{\mathcal{Z}}$ of switching bilateral constraints

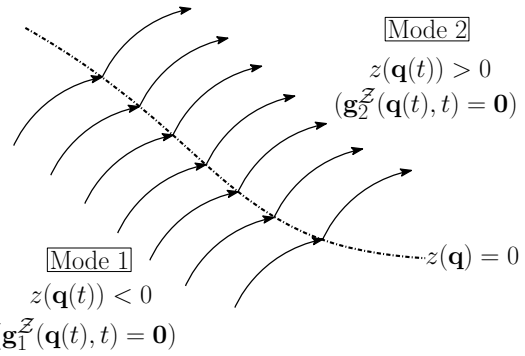

Figure 1: Illustration of smooth dynamical modes 1 and 2, and the possible flow of the equations of motion crossing the switching surface $z(\mathbf{q}) = 0$.

$$\mathbf{g}^{\mathcal{Z}}(\mathbf{q}(t), t) = \mathbf{0}, \tag{1}$$

where $\mathbf{q}(t) \in \mathbb{R}^n$ represents the coordinates. These constraint expressions instantaneously change with respect to state-dependent conditional statements, also called switching functions, that partition $\mathbb{R}^n$ into several open domains. These switching functions define switching surfaces, that play a vital role in our modelling framework. The *constraint space* is the set of all $\mathbf{q}(t) \in \mathbb{R}^n$ which satisfy the constraint equation in Eq. (1). It is a subspace of $\mathbb{R}^n$, but it is not a smooth manifold because of the switching conditions.

In this section, let us first introduce the formulation of bilateral constraints orchestrated by one switching surface, and further generalize to multiple surfaces.

2.1 Single switching surface

Let us consider a single *switching surface* which is defined by all $\mathbf{q}(t) \in \mathbb{R}^n$ such that

$$z(\mathbf{q}) = 0, \tag{2}$$

where the function $z(\mathbf{q}) : \mathbb{R}^n \to \mathbb{R}$ is the so-called *switching function*.

The function $z(\mathbf{q})$ shall govern the bilateral constraint $\mathbf{g}^{\mathcal{Z}}(\mathbf{q}(t), t) = \mathbf{0}$, and the surface $z(\mathbf{q}) = 0$ punctuates the system dynamics into two continuous or smooth modes 1 and 2 defined by $z(\mathbf{q}(t)) < 0$ and $z(\mathbf{q}(t)) > 0$ respectively, as illustrated in Figure 1. As the state travels across the switching surface $z(\mathbf{q}) = 0$, the geometry of the constraint space defined by Eq. (1) may exhibit some nonsmoothness. The state-dependent switching constraints are thus represented in a conditional form as

$$\mathbf{g}^{\mathcal{Z}}(\mathbf{q}(t), t) = \begin{cases} \mathbf{g}_1^{\mathcal{Z}}(\mathbf{q}(t), t) = \mathbf{0} & \text{if } z(\mathbf{q}(t)) < 0, \\ \dfrac{1}{2}(\mathbf{g}_1^{\mathcal{Z}}(\mathbf{q}(t), t) + \mathbf{g}_2^{\mathcal{Z}}(\mathbf{q}(t), t)) = \mathbf{0} & \text{if } z(\mathbf{q}) = 0, \\ \mathbf{g}_2^{\mathcal{Z}}(\mathbf{q}(t), t) = \mathbf{0} & \text{if } z(\mathbf{q}(t)) > 0, \end{cases} \tag{3}$$

where the functions $\mathbf{g}_1^{\mathcal{Z}}(\mathbf{q}(t), t)$ and $\mathbf{g}_2^{\mathcal{Z}}(\mathbf{q}(t), t)$ are assumed to be sufficiently smooth and differentiable.

Alternatively, we can reformulate Eq. (3) to combine the pre- and post-switch constraints $\mathbf{g}_1^{\mathcal{Z}}(\mathbf{q}(t), t)$ and $\mathbf{g}_2^{\mathcal{Z}}(\mathbf{q}(t), t)$ along with the switching function $z(\mathbf{q})$ into a generalized algebraic form as

$$\mathbf{g}^{\mathcal{Z}}(\mathbf{q}(t), t) = (1 - s^+(z(\mathbf{q}))\mathbf{g}_1^{\mathcal{Z}}(\mathbf{q}(t), t) + s^+(z(\mathbf{q}))\mathbf{g}_2^{\mathcal{Z}}(\mathbf{q}(t), t) = \mathbf{0}, \tag{4}$$

where the switching function $z(\mathbf{q})$ is now orchestrated by the Heaviside step function $s^+(\bullet)$ as shown in Figure 2 and defined as

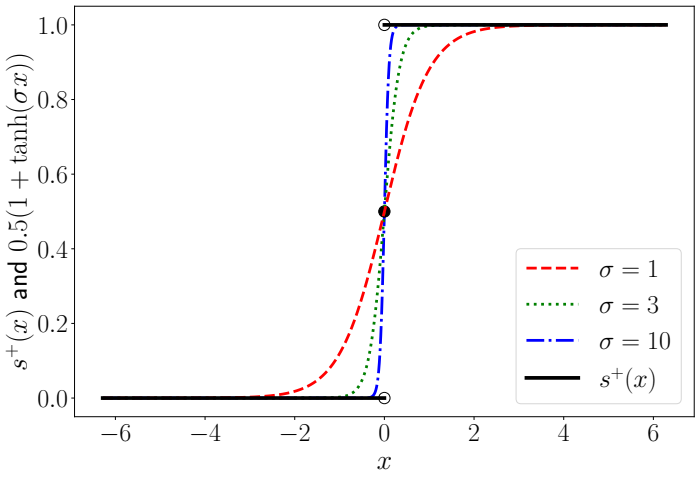

Figure 2: Hyperbolic tangent approximation $s^+(x) \simeq 0.5(1+\tanh(\sigma x))$ of the Heaviside step function $s^+(x)$.

$$s^+(x) = \begin{cases} 1 & \text{if } x \geq 0, \\ 1/2 & \text{if } x = 0, \\ 0 & \text{if } x < 0. \end{cases} \tag{5}$$

However, classical DAE solvers rely on continuity and differentiability of $\mathbf{g}^{\mathcal{Z}}(\mathbf{q}(t), t)$. These requirements are satisfied in the modes $z(\mathbf{q}(t)) < 0$ and $z(\mathbf{q}(t)) > 0$, but not necessarily at $z(\mathbf{q}) = 0$. Due to discontinuities introduced by $s^+(x)$ at $x = 0$, numerical difficulties are expected along the switching surface $z(\mathbf{q}) = 0$.

In this regard, smooth approximations of $s^+(x)$ are sometimes performed, e.g., using the hyperbolic tangent function as shown in Figure 2. Indeed, we have

$$s^+(x) = \lim_{\sigma \to \infty} \frac{1}{2}(1 + \tanh(\sigma x)). \tag{6}$$

Unfortunately, the smoothing parameter σ considerably influences the solution. For low values of σ, the resulting constraints will deviate from the exact constraints, and as σ increases, the sharp transitions will induce high numerical stiffness resulting in a stiff system of equations. In this paper, such smooth approximations are therefore not considered.

In the field of nonsmooth dynamics and switched DAEs, several methods have been proposed to handle the discontinuities induced by $s^+(x)$. For instance, the value of $s^+(x)$ at $x = 0$ can be specified by a convex relaxation of switching constraints, that relies on a set-valued Heaviside step function [24, 30] $S^+(\bullet)$ defined as

$$S^+(x) = \begin{cases} \{1\} & \text{if } x > 0, \\ [0, 1] & \text{if } x = 0, \\ \{0\} & \text{if } x < 0. \end{cases} \tag{7}$$

Other relaxation methods such as closed convex hull (CCH) or switching constraint connected (SCC) as proposed in [24] may also be considered.

However, in the context of this paper, convex relaxation methods are less relevant because $\mathbf{g}_1^{\mathcal{Z}}(\mathbf{q}(t), t)$ and $-\mathbf{g}_1^{\mathcal{Z}}(\mathbf{q}(t), t)$ represent the same constraint space. Therefore, non-convex combinations of $\mathbf{g}_1^{\mathcal{Z}}(\mathbf{q}(t), t)$ and $\mathbf{g}_2^{\mathcal{Z}}(\mathbf{q}(t), t)$ have the same legitimity as convex ones, and there is no strong argument to limit oneself to convex approximations.

2.1.1 Definition of the switching surface

It is noteworthy that the switching surface $z(\mathbf{q}) = 0$ plays a crucial role in the modelling framework. In particular, $z(\mathbf{q}) = 0$ orchestrates the geometry of the constraint space across the switching interface. Let use a motivating 2D example to illustrate this concept. This example shall also serve as a benchmark test throughout the paper.

Motivating example: consider a material point which evolves on a nonsmooth track defined by two intersecting linear portions as shown in Figure 3. Let θ be the kink angle between the two portions. In the coordinate system

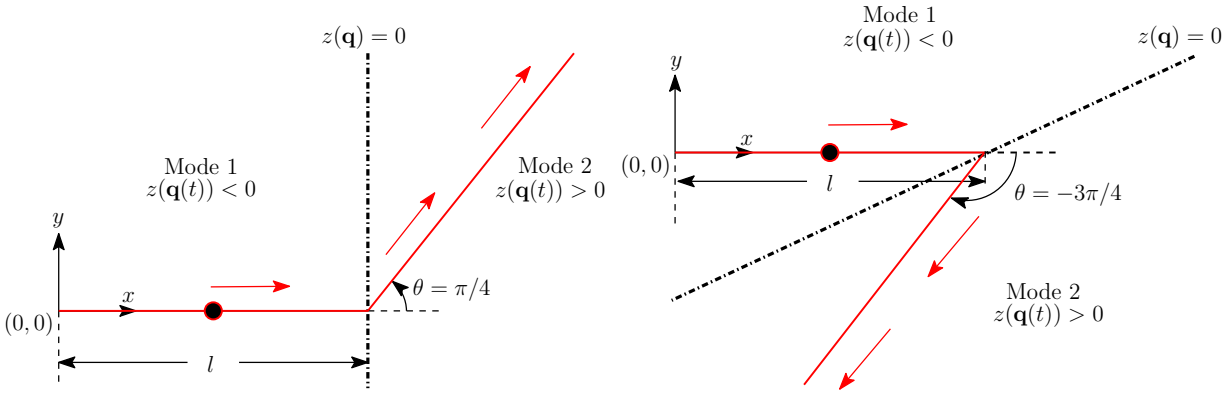

(a) Case 1 ($\theta = \pi/4$) : the switching function can be defined as $z(\mathbf{q}) = x - l$.

(b) Case 2 ($\theta = -3\pi/4$) : the switching function can be defined as $z(\mathbf{q}) = -y + \tan\theta/2(x - l)$.

Figure 3: Material point on a nonsmooth track represented in red solid line. The track defines the constraint space. Depending on the kink angle, different switching functions can be considered.

shown in Figure 3, the position of the point is defined by $\mathbf{q}(t) = \begin{bmatrix} x(t) & y(t) \end{bmatrix}^T \in \mathbb{R}^2$, and is subjected to one algebraic constraint $g^{\mathcal{Z}}(\mathbf{q}(t)) = 0 \in \mathbb{R}^1$, i.e., $m^{\mathcal{Z}} = 1$. The initial position of the point is defined for $t = 0$ as $x(0) = y(0) = 0$, and a consistent initial velocity $\dot{x}(0) = v_x$ and $\dot{y}(0) = 0$ is imposed. The intersection point is localized at $x = l$, $y = 0$. The scalar constraint $g^{\mathcal{Z}}(\mathbf{q}(t)) = 0$ is defined by Eq. (3) (or Eq. (4)) with the functions

$$g_1^{\mathcal{Z}}(\mathbf{q}(t)) = y(t), \tag{8}$$

$$g_2^{\mathcal{Z}}(\mathbf{q}(t)) = y(t) - \tan\theta(x(t) - l). \tag{9}$$

Two cases are considered. In case 1, let us consider $\theta = \pi/4$ and a choice of switching function as

$$z(\mathbf{q}) = x - l. \tag{10}$$

In case 2, let us consider $\theta = -3\pi/4$ and a choice of switching function as

$$z(\mathbf{q}) = -y + \frac{\tan\theta}{2}(x - l). \tag{11}$$

As $\tan(\pi/4) = \tan(-3\pi/4)$, the expression of $g_1^{\mathcal{Z}}(\mathbf{q}(t))$ and $g_2^{\mathcal{Z}}(\mathbf{q}(t))$ in Eqs. (8) and (9) is strictly identical in the two cases. The two cases solely differ by the definition of the switching surface, which selects the constraint according to the position $\mathbf{q}(t)$. Thus in conclusion, we can state that the definition of the switching surface $z(\mathbf{q}) = 0$ controls the geometry of the constraint space. Numerical results presented in Section 5 will further validate this proposition.

Let us formalize the requirements for the definition of the switching function in a general setting. Firstly and obviously, the two portions of the constraint space should intersect at the switching surface. This means that $\forall \mathbf{q}(t)$ satisfying both $\mathbf{g}_1^{\mathcal{Z}}(\mathbf{q}(t), t) = \mathbf{0}$ and $z(\mathbf{q}) = 0$, we require $\mathbf{g}_2^{\mathcal{Z}}(\mathbf{q}(t), t) = \mathbf{0}$. Conversely, $\forall \mathbf{q}(t)$ satisfying both $\mathbf{g}_2^{\mathcal{Z}}(\mathbf{q}(t), t) = \mathbf{0}$ and $z(\mathbf{q}) = 0$, we require $\mathbf{g}_1^{\mathcal{Z}}(\mathbf{q}(t), t) = \mathbf{0}$. In this way, we ensure that the switching between $\mathbf{g}_1^{\mathcal{Z}}(\mathbf{q}(t), t)$ and $\mathbf{g}_2^{\mathcal{Z}}(\mathbf{q}(t), t)$ is well-defined at the switching surface $z(\mathbf{q}) = 0$.

It is also clear from Figure 4, that the switching surface $z(\mathbf{q}) = x - l = 0$ cannot be tangent to the constraint space. This implies that the gradients of pre- and post-switching constraints denoted as $\mathbf{G}_1^{\mathcal{Z}}(\mathbf{q}(t)) = \partial g_1^{\mathcal{Z}}(\mathbf{q}(t))/\partial \mathbf{q}(t) = [0, 1]$ and $\mathbf{G}_2^{\mathcal{Z}}(\mathbf{q}(t)) = \partial g_2^{\mathcal{Z}}(\mathbf{q}(t))/\partial \mathbf{q}(t) = [-\tan(\theta), 1]$, and the gradient of the switching surface $\mathbf{Z}(\mathbf{q}) = \partial z(\mathbf{q})/\partial \mathbf{q}$ should be linearly independent. In a general setting, the switching function $z(\mathbf{q}) : \mathbb{R}^n \to \mathbb{R}$ should be such that the matrices

$$\begin{bmatrix} \mathbf{G}_1^{\mathcal{Z}}(\mathbf{q}(t), t) \\ \mathbf{Z}(\mathbf{q}(t)) \end{bmatrix} \text{ and } \begin{bmatrix} \mathbf{G}_2^{\mathcal{Z}}(\mathbf{q}(t), t) \\ \mathbf{Z}(\mathbf{q}(t)) \end{bmatrix} \tag{12}$$

are full rank on the switching surface $z(\mathbf{q}) = 0$.

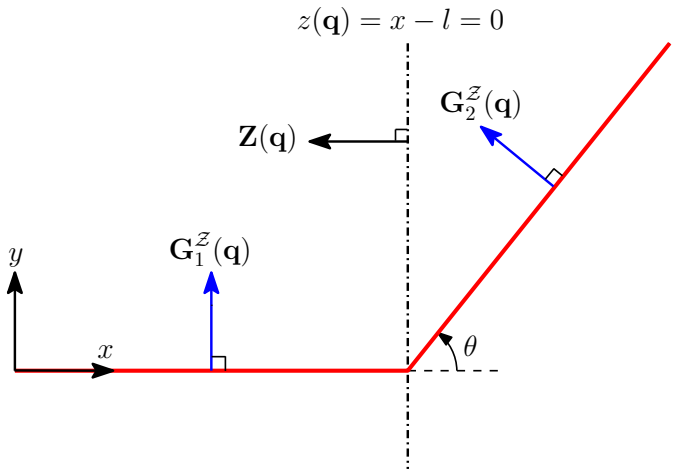

Figure 4: Linear independence of pre and post-switch gradients $\mathbf{G}_1^{\mathcal{Z}}(\mathbf{q})$ and $\mathbf{G}_2^{\mathcal{Z}}(\mathbf{q})$ and the gradient of switching surface $\mathbf{Z}(\mathbf{q})$.

2.2 Constraints at velocity level

We now take the formulation of constraints at the velocity level, as the velocities $\dot{\mathbf{q}}(t)$ should also be compatible with the constraints. In the smooth phases of motion $z(\mathbf{q}(t)) < 0$ and $z(\mathbf{q}(t)) > 0$, a first time differentiation of the constraint in Eq. (4) results in the constraints at velocity level

$$\dot{\mathbf{g}}^{\mathcal{Z}}(\mathbf{q}(t), t) = \mathbf{G}^{\mathcal{Z}}(\mathbf{q}(t), t)\dot{\mathbf{q}}(t) + \mathbf{g}_t^{\mathcal{Z}}(\mathbf{q}(t), t) = \mathbf{0}, \tag{13}$$

where $\mathbf{G}^{\mathcal{Z}}(\mathbf{q}(t), t) = \partial \mathbf{g}^{\mathcal{Z}}(\mathbf{q}(t), t)/\partial \mathbf{q}(t) \in \mathbb{R}^{m^{\mathcal{Z}} \times n}$ is the constraint gradient, and the term $\mathbf{g}_t^{\mathcal{Z}}(\mathbf{q}(t), t) = \partial \mathbf{g}^{\mathcal{Z}}(\mathbf{q}(t), t)/\partial t$.

In the smooth modes, the constraint gradient is defined in a standard manner, but this definition does not hold at the switching surface $z(\mathbf{q}) = 0$ because of the lack of differentiability of the step function. In particular, if $z(\mathbf{q}(t)) < 0$ for $t < t_i$ and $z(\mathbf{q}(t)) > 0$ for $t > t_i$, then the left and right limits exist at t_i (as a consequence of the differentiability of $\mathbf{g}_1^{\mathcal{Z}}(\mathbf{q}(t), t)$ and $\mathbf{g}_2^{\mathcal{Z}}(\mathbf{q}(t), t)$), but have different values as

$$\mathbf{G}^{\mathcal{Z}+}(\mathbf{q}(t_i), t_i) = \lim_{\gamma \to t_i,\, \gamma > t_i} \mathbf{G}^{\mathcal{Z}}(\mathbf{q}(\gamma), \gamma) = \mathbf{G}_2^{\mathcal{Z}}(\mathbf{q}(t_i), t_i), \tag{14}$$

$$\mathbf{G}^{\mathcal{Z}-}(\mathbf{q}(t_i), t_i) = \lim_{\gamma \to t_i,\, \gamma < t_i} \mathbf{G}^{\mathcal{Z}}(\mathbf{q}(\gamma), \gamma) = \mathbf{G}_1^{\mathcal{Z}}(\mathbf{q}(t_i), t_i). \tag{15}$$

In the above expression, we considered a situation where the system switches from mode 1 to mode 2.

Notice that at the switching surface $z(\mathbf{q}) = 0$, we have an indeterminacy in the constraint gradient $\mathbf{G}^{\mathcal{Z}}$, as one may consider $\mathbf{G}^{\mathcal{Z}} = \mathbf{G}_1^{\mathcal{Z}}$, or $\mathbf{G}^{\mathcal{Z}} = \mathbf{G}_2^{\mathcal{Z}}$, or an intermediate value between both.

In the special case when the motion is fully-constrained, $\mathbf{G}^{\mathcal{Z}}(\mathbf{q}(t), t)$ is a square matrix. In this case, assuming that $\mathbf{G}_1^{\mathcal{Z}}(\mathbf{q}(t), t)$ and $\mathbf{G}_2^{\mathcal{Z}}(\mathbf{q}(t), t)$ are invertible, the velocities $\dot{\mathbf{q}}(t)$ can be evaluated in the smooth modes as $\dot{\mathbf{q}}(t) = -(\mathbf{G}^{\mathcal{Z}})^{-1}(\mathbf{q}(t), t)\mathbf{g}_t^{\mathcal{Z}}(\mathbf{q}(t), t)$. At the switching surface $z(\mathbf{q}) = 0$, velocities $\dot{\mathbf{q}}(t_i)$ are discontinuous but the left $\dot{\mathbf{q}}^-(t_i)$ and right $\dot{\mathbf{q}}^+(t_i)$ limits exist as

$$\dot{\mathbf{q}}^+(t_i) = \lim_{\gamma \to t_i,\, \gamma > t_i} \dot{\mathbf{q}}(\gamma), \tag{16a}$$

$$= -(\mathbf{G}_2^{\mathcal{Z}})^{-1}(\mathbf{q}(t_i), t_i)\mathbf{g}_{2t}^{\mathcal{Z}}(\mathbf{q}(t_i), t_i), \tag{16b}$$

$$\dot{\mathbf{q}}^-(t_i) = \lim_{\gamma \to t_i,\, \gamma < t_i} \dot{\mathbf{q}}(\gamma), \tag{17a}$$

$$= -(\mathbf{G}_1^{\mathcal{Z}})^{-1}(\mathbf{q}(t_i), t_i)\mathbf{g}_{1t}^{\mathcal{Z}}(\mathbf{q}(t_i), t_i). \tag{17b}$$

and have different values. Therefore, the velocity jump is defined by $\dot{\mathbf{q}}^+(t_i) - \dot{\mathbf{q}}^-(t_i)$.

2.3 Constraints at acceleration level

We take the formulation of constraints at the acceleration level, as the accelerations $\ddot{\mathbf{q}}(t)$ should also be compatible with the constraints. In the smooth phases of motion $z(\mathbf{q}(t)) < 0$ and $z(\mathbf{q}(t)) > 0$, a second time differentiation of the constraint in Eq. (4) result in the constraint at acceleration level

$$\ddot{\mathbf{g}}^{\mathcal{Z}}(\mathbf{q}(t), t) = \mathbf{G}^{\mathcal{Z}}(\mathbf{q}(t), t)\ddot{\mathbf{q}}(t) + \dot{\mathbf{G}}^{\mathcal{Z}}(\mathbf{q}(t), \dot{\mathbf{q}}(t), t)\dot{\mathbf{q}}(t) + \dot{\mathbf{g}}_t^{\mathcal{Z}}(\mathbf{q}(t), \dot{\mathbf{q}}(t), t) = \mathbf{0}. \tag{18}$$

In the smooth modes, the accelerations $\ddot{\mathbf{q}}(t)$ can be evaluated in a standard manner, but this definition does not hold at the switching surface $z(\mathbf{q}) = 0$. As velocities $\dot{\mathbf{q}}(t)$ undergo jumps, the accelerations $\ddot{\mathbf{q}}(t)$ are defined almost everywhere. This implies that the accelerations $\ddot{\mathbf{q}}(t)$ are not defined at the switching surface $z(\mathbf{q}) = 0$.

2.4 Multiple switching surfaces

We further extend the formulation of switching bilateral constraints $\mathbf{g}^{\mathcal{Z}}(\mathbf{q}(t), t) = \mathbf{0}$ that are punctuated by multiple switching surfaces. Let us denote k as the number of switching surfaces.

First of all, for the case of a single switching surface, i.e., $k = 1$, we can define $z_1(\mathbf{q}) = -z(\mathbf{q})$, and $z_2(\mathbf{q}) = +z(\mathbf{q})$, and consider that $\mathbb{R}^n$ is partitioned into two disjoint sets as

$$\mathcal{X}_i = \{\mathbf{q}(t) \in \mathbb{R}^n \mid z_i(\mathbf{q}) > 0\}, \tag{19}$$

where $i = 1, 2$.

Then the generalized constraint in Eq. (4) can be rewritten as

$$\mathbf{g}^{\mathcal{Z}}(\mathbf{q}(t), t) = (1 - s^+(z_2(\mathbf{q})))s^+(z_1(\mathbf{q}))\mathbf{g}_1^{\mathcal{Z}}(\mathbf{q}(t), t) + (1 - s^+(z_1(\mathbf{q})))s^+(z_2(\mathbf{q}))\mathbf{g}_2^{\mathcal{Z}}(\mathbf{q}(t), t). \tag{20}$$

Now we consider a dynamical system, with a number of k switching surfaces. In this case, the system dynamics is separated into $k + 1$ dynamical modes. Each mode i corresponds to a set $\mathcal{X}_i \subset \mathbb{R}^n$ defined as in Eq. (19), and based on the function $z_i(\mathbf{q})$ with $i = 1, \cdots, k + 1$. Following the approach proposed in [24, 31], the switching constraints and their conditional statements are thus unified into a generalized algebraic form as

$$\mathbf{g}^{\mathcal{Z}}(\mathbf{q}(t), t) = \sum_{i=1}^{k+1} \left(\prod_{j \neq i} (1 - s^+(z_j(\mathbf{q}(t)))) \right) s^+(z_i(\mathbf{q}(t)))\mathbf{g}_i^{\mathcal{Z}}(\mathbf{q}(t), t) = \mathbf{0}. \tag{21}$$

The partitioning of $\mathbb{R}^n$ into sets $\mathcal{X}_i$ should be performed in a meaningful and non-overlapping manner. Thus, the following partition properties should be satisfied

- *Global coverage of* $\mathbb{R}^n$*:* $\bigcup_i \overline{\mathcal{X}}_i = \mathbb{R}^n$, where $\overline{\mathcal{X}}_i$ is the closure of $\mathcal{X}_i$,
- *Non-empty interior:* $\text{int}(\mathcal{X}_i) \neq \emptyset, \quad \forall i$,
- *Disjoint boundaries:* $\partial\mathcal{X}_i \cap \partial\mathcal{X}_j = \emptyset$, for $i \neq j$, where $\partial\mathcal{X}_i$ represents the boundary of $\mathcal{X}_i$.

For the sake of conciseness, we do not present the constraints at velocity level $\dot{\mathbf{g}}^{\mathcal{Z}}(\mathbf{q}(t), t) = \mathbf{0}$ and acceleration level $\ddot{\mathbf{g}}^{\mathcal{Z}}(\mathbf{q}(t), t) = \mathbf{0}$ in the general case, but they are similarly obtained by first and second time differentiation of Eq. (21) as presented in Sections 2.2 and 2.3.

3 Equations of motion

The equations of motion for multibody systems subjected to non-differentiable bilateral constraints can either be expressed as hybrid differential-algebraic equations (HDAEs), or be based on an equality of differential measures. In this section, we present both forms, which further lend themselves to a particular choice of the time integration scheme.

3.1 Hybrid differential-algebraic equation

A hybrid form of the equations of motion (HDAEs) involves a continuous-time set of differential equations, and a finite automaton that defines the behaviour of the system at switching. In our context, the HDAE shall involve: (i) a standard DAE set of equations that holds in the smooth modes, and (ii) a set of impact equations that exclusively defines the switching dynamics, and thus holds at the switching surfaces.

For almost every time, the equations of motion of a multibody system with non-differentiable switching constraints takes the standard index-3 DAE form

$$\dot{\mathbf{q}}(t) = \mathbf{v}(t), \tag{22}$$

$$\mathbf{M}(\mathbf{q}(t))\dot{\mathbf{v}}(t) + \mathbf{G}^T(\mathbf{q}(t), t)\boldsymbol{\lambda}(t) = \mathbf{f}(\mathbf{q}(t), \mathbf{v}(t), t), \tag{23}$$

$$\mathbf{g}(\mathbf{q}(t), t) = \mathbf{0}. \tag{24}$$

In these equations,

- $\mathbf{g}(\mathbf{q}(t), t) \in \mathbb{R}^m$ with $m = m^{\mathcal{Z}} + m^{\overline{\mathcal{Z}}}$ is the set of bilateral constraints, which includes the switching (generalized) constraint $\mathbf{g}^{\mathcal{Z}}(\mathbf{q}(t), t) \in \mathbb{R}^{m^{\mathcal{Z}}}$ defined in Eq. (21), and its complementary set, i.e., the set of smooth constraints $\mathbf{g}^{\overline{\mathcal{Z}}}(\mathbf{q}(t), t) \in \mathbb{R}^{m^{\overline{\mathcal{Z}}}}$. The full set of constraints $\mathcal{C} = \mathcal{Z} \bigcup \overline{\mathcal{Z}}$ is

$$\mathbf{g}(\mathbf{q}(t), t) = \begin{bmatrix} \mathbf{g}^{\overline{\mathcal{Z}}}(\mathbf{q}(t), t) \\ \mathbf{g}^{\mathcal{Z}}(\mathbf{q}(t), t) \end{bmatrix}. \tag{25}$$

- Further, $\mathbf{G}(\mathbf{q}(t), t) \in \mathbb{R}^{m \times n}$ is the matrix of constraint gradient, and $\boldsymbol{\lambda}(t) \in \mathbb{R}^m$ is the set of Lagrange multipliers such that

$$\mathbf{G}(\mathbf{q}(t), t) = \begin{bmatrix} \mathbf{G}^{\overline{\mathcal{Z}}}(\mathbf{q}(t), t) \\ \mathbf{G}^{\mathcal{Z}}(\mathbf{q}(t), t) \end{bmatrix}, \qquad \boldsymbol{\lambda}(t) = \begin{bmatrix} \boldsymbol{\lambda}^{\overline{\mathcal{Z}}}(t) \\ \boldsymbol{\lambda}^{\mathcal{Z}}(t) \end{bmatrix}. \tag{26}$$

- The term $\mathbf{G}^T(\mathbf{q}(t), t)\boldsymbol{\lambda}(t)$ in Eq. (23) denotes the constraint reaction force,

- $\mathbf{q}(t) \in \mathbb{R}^n$ denotes the generalized coordinates,

- $\mathbf{v}(t) \in \mathbb{R}^n$ denotes the generalized velocities,

- $\mathbf{M}(\mathbf{q}(t)) \in \mathbb{R}^{n \times n}$ is the symmetric positive semi-definite mass matrix,

- $\mathbf{f}(\mathbf{q}(t), \mathbf{v}(t), t) \in \mathbb{R}^n$ is the resultant of gyroscopic, and other forces and torques.

The initial conditions shall take the form $\mathbf{q}(t_0) = \mathbf{q}_0$ and $\dot{\mathbf{q}}(t_0) = \dot{\mathbf{q}}_0$.

On the switching surfaces, one cannot describe the dynamics based on Eqs. (22-24) for the following reasons. Firstly, the value of $\mathbf{G}$ is not determinate at the switching surface. For instance as illustrated in Figure 5, the reaction force may be assumed to be along the direction of pre-switch gradient $\mathbf{G}^-$, or along the post-switch gradient $\mathbf{G}$, or along an intermediate gradient such as the bisector. In addition, the reaction force is expected to be impulsive at the switching surface, as the velocities $\dot{\mathbf{q}}(t_i)$ may be discontinuous. This means that an additional set of equations should be introduced to describe the behaviour on the switching surface. The switching dynamics is thus expressed by the impact equation which involves the velocity constraint

$$\mathbf{M}(\mathbf{q}(t_i))(\mathbf{v}(t_i) - \mathbf{v}^-(t_i)) + \mathbf{R} = \mathbf{0}, \tag{27}$$

$$\mathbf{G}(\mathbf{q}(t_i), t_i)\mathbf{v}(t_i) = -\mathbf{g}_t(\mathbf{q}(t_i), t_i), \tag{28}$$

with the short notation $\mathbf{v}(t_i) = \mathbf{v}^+(t_i)$ and $\mathbf{G}(\mathbf{q}(t_i), t_i) = \mathbf{G}^+(\mathbf{q}(t_i), t_i)$, and where $\mathbf{R}$ is the impulse of the constraint reaction force.

In order to obtain a complete impact model, we may introduce an additional assumption on the direction of $\mathbf{R}$ based on the knowledge of $\mathbf{G}^-(\mathbf{q}(t_i), t_i)$ and $\mathbf{G}(\mathbf{q}(t_i), t_i)$. For that purpose, we can construct an intermediate

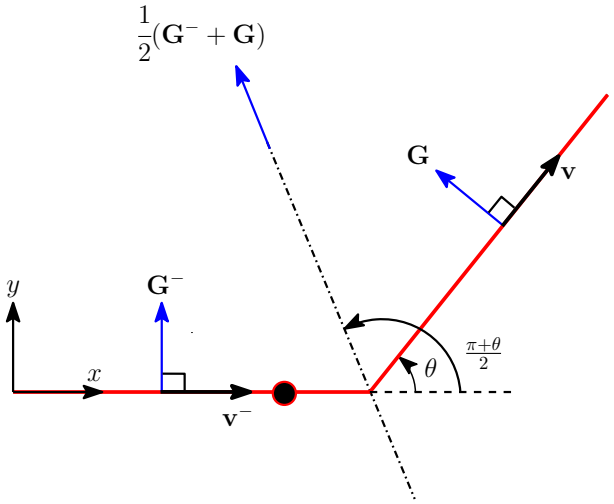

Figure 5: Possible models for the direction of reaction force at switching surface: along the pre-switch gradient $\mathbf{G}^-$, along the post-switch gradient $\mathbf{G}$, or along an intermediate gradient such as the bisector.

constraint gradient $\mathbf{G}_\mathcal{E}$ by interpolation between $\mathbf{G}^-(\mathbf{q}(t_i), t_i)$ and $\mathbf{G}(\mathbf{q}(t_i), t_i)$. For instance, one may be tempted to consider the interpolation formula

$$\mathbf{G}_\mathcal{E} = (1 - \mathcal{E})\mathbf{G}^-(\mathbf{q}(t_i), t_i) + \mathcal{E}\mathbf{G}(\mathbf{q}(t_i), t_i), \tag{29}$$

where $\mathcal{E} \in [0, 1]$ is the interpolation parameter. Unfortunately, this formula is not applicable in general, and we will see that more sophisticated interpolation schemes should be considered. Let us simply accept for the moment that an intermediate gradient $\mathbf{G}_\mathcal{E}$ is specified in the model. Then, we assume that $\mathbf{R}$ is expressed as

$$\mathbf{R} = \mathbf{G}_\mathcal{E}^T \mathbf{\Lambda}. \tag{30}$$

In summary, the impact model is

$$\mathbf{M}(\mathbf{q}(t_i))(\mathbf{v}(t_i) - \mathbf{v}^-(t_i)) + \mathbf{G}_\mathcal{E}^T \mathbf{\Lambda} = \mathbf{0}, \tag{31}$$

$$\mathbf{G}(\mathbf{q}(t_i), t_i)\mathbf{v}(t_i) = -\mathbf{g}_t(\mathbf{q}(t_i), t_i). \tag{32}$$

3.2 Equality of differential measures

The HDAE form is based on two sets of equations: the DAE form in Eqs. (22-24), and the impact equation in Eqs. (31-32). Alternatively, the equations of motion can be expressed in terms of differential measures as follows

$$\dot{\mathbf{q}}(t) = \mathbf{v}(t), \tag{33}$$

$$\mathbf{M}(\mathbf{q}(t))\mathrm{d}\mathbf{v} - \mathbf{G}_\mathcal{E}^T \mathrm{d}\mathbf{i} = \mathbf{f}(\mathbf{q}(t), \mathbf{v}(t), t)\mathrm{d}t, \tag{34}$$

$$\mathbf{g}(\mathbf{q}(t), t) = \mathbf{0}. \tag{35}$$

This unique set of equations holds in the smooth modes, and also at the switching surfaces. In Eq. (34), $\mathbf{G}_\mathcal{E}$ is the intermediate gradient between $\mathbf{G}^-(\mathbf{q}(t_i), t_i)$ and $\mathbf{G}(\mathbf{q}(t_i), t_i)$, as discussed in the previous section. Notice that in the smooth modes, $\mathbf{G}_\mathcal{E} = \mathbf{G}^-(\mathbf{q}(t_i), t_i) = \mathbf{G}(\mathbf{q}(t_i), t_i)$. Equations (33-35) are subjected to initial conditions $\mathbf{q}(t_0) = \mathbf{q}_0$ and $\dot{\mathbf{q}}(t_0) = \dot{\mathbf{q}}_0$.

Equation (34) is defined as an equality of differential measures. In this equation, $\mathrm{d}\mathbf{i}$ is the impulse measure of the constraint reaction forces, $\mathrm{d}\mathbf{v}$ is the differential measure associated with velocity $\mathbf{v}(t)$, and $\mathrm{d}t$ is the Lebesgue measure. Neglecting singular measures, the measures $\mathrm{d}\mathbf{v}$ and $\mathrm{d}\mathbf{i}$ can be decomposed as

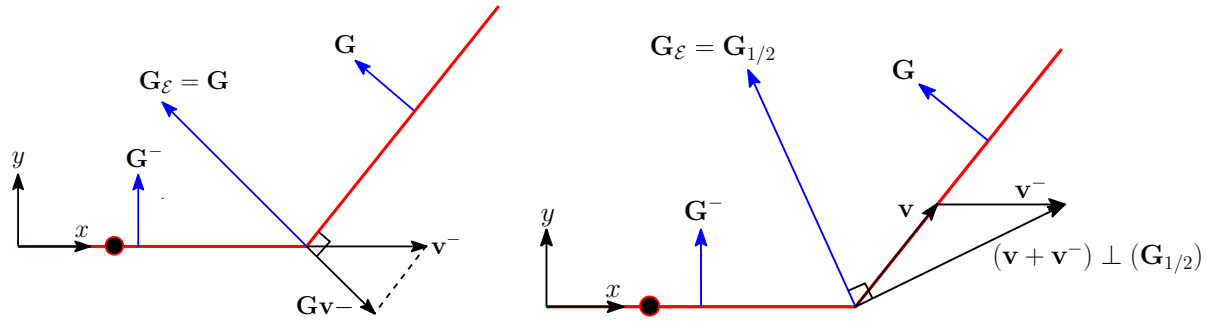

(a) Choice of $\mathbf{G}_\mathcal{E}$ as post-switch gradient. $\mathbf{G}\mathbf{v}^-$ is the component of $\mathbf{v}^-$ orthogonal to the post-switch constraint.

(b) Choice of $\mathbf{G}_\mathcal{E}$ as bisector between the gradients $\mathbf{G}^-$ and $\mathbf{G}$ and the property of orthogonality $\mathbf{G}_{1/2}(\mathbf{v}+\mathbf{v}^-) = 0$.

Figure 6: Choice of constraint gradient at switching surface.

$$\mathrm{d}\mathbf{v} = \dot{\mathbf{v}}\mathrm{d}t + \sum_i (\mathbf{v}(t_i) - \mathbf{v}^-(t_i))\mathrm{d}\delta_{t_i}, \tag{36}$$

$$\mathrm{d}\mathbf{i} = \boldsymbol{\lambda}\mathrm{d}t + \sum_i \mathbf{p}_i \mathrm{d}\delta_{t_i}, \tag{37}$$

where $\mathbf{p}_i$ is the impulse (percussion) at switching computed at t_i, and $\mathrm{d}\delta_{t_i}$ is the Dirac delta supported at t_i as

$$\int_{(t_1,t_2]} \mathrm{d}\delta_{t_i} = \begin{cases} 1, & \text{if } t_i \in (t_1,t_2], \\ 0, & \text{if } t_i \notin (t_1,t_2]. \end{cases} \tag{38}$$

Introducing Eqs. (36-37) into Eqs. (33-35) leads to: (i) the standard DAE form of the equations of motion as stated in Eqs. (22-24) for almost every time, and (ii) to an impact equation at the switching time t_i as defined in Eqs. (31-32).

3.3 Analysis of the impact model

In this section, we study the impact model, and in particular the influence of the choice of $\mathbf{G}_\mathcal{E}$ on the energy behaviour at switching. Let us drop the functional arguments of the different variables for the sake of notational simplicitly. The analysis is restricted to scleronomic systems (the constraints do not explicitly depend on time) with an invertible mass matrix. We obtain from Eq. (31)

$$\mathbf{v} = \mathbf{v}^- - \mathbf{M}^{-1}\mathbf{G}_\mathcal{E}^T\boldsymbol{\Lambda}. \tag{39}$$

Substituting in Eq. (32), we obtain

$$\mathbf{G}\mathbf{v}^- - \mathbf{G}\mathbf{M}^{-1}\mathbf{G}_\mathcal{E}^T\boldsymbol{\Lambda} = \mathbf{0}. \tag{40}$$

Defining $\mathbf{D}_\mathcal{E} = \mathbf{G}\mathbf{M}^{-1}\mathbf{G}_\mathcal{E}^T$, we obtain,

$$\boldsymbol{\Lambda} = \mathbf{D}_\mathcal{E}^{-1}\mathbf{G}\mathbf{v}^-. \tag{41}$$

Notice that if $\mathbf{G}_\mathcal{E} = \mathbf{G}$, $\mathbf{D}_\mathcal{E}$ is symmetric and coincides with the classical Delassus operator $\mathbf{D} = \mathbf{G}\mathbf{M}^{-1}\mathbf{G}^T$. But if $\mathbf{G}_\mathcal{E} \neq \mathbf{G}$, $\mathbf{D}_\mathcal{E}$ is not symmetric. Further we evaluate the change in energy as

$$E - E^- = \frac{1}{2}(\mathbf{v})^T\mathbf{M}\mathbf{v} - \frac{1}{2}(\mathbf{v}^-)\mathbf{M}\mathbf{v}^-, \tag{42a}$$
$$= \frac{1}{2}(\mathbf{v} + \mathbf{v}^-)^T\mathbf{M}(\mathbf{v} - \mathbf{v}^-), \tag{42b}$$
$$= -\frac{1}{2}(\mathbf{v} + \mathbf{v}^-)^T\mathbf{G}_\mathcal{E}^T\mathbf{\Lambda}, \tag{42c}$$
$$= -\frac{1}{2}\mathbf{\Lambda}^T\mathbf{G}_\mathcal{E}(\mathbf{v} + \mathbf{v}^-), \tag{42d}$$
$$= -\frac{1}{2}(\mathbf{v}^-)^T\mathbf{G}^T\mathbf{D}_\mathcal{E}^{-T}\mathbf{G}_\mathcal{E}(\mathbf{v} + \mathbf{v}^-). \tag{42e}$$

These developments are valid for any choice of $\mathbf{G}_\mathcal{E}$. To go deeper in the analysis, we need to exploit a more precise expression of $\mathbf{G}_\mathcal{E}$, which was not specified yet. As the definition of $\mathbf{G}_\mathcal{E}$ by interpolation is not trivial in the general case, we continue the developments in two special cases.

3.3.1 Special choice: $\mathbf{G}_\mathcal{E} = \mathbf{G}$

As a special case, let us consider the definition of the intermediate gradient as the post-switch gradient $\mathbf{G}_\mathcal{E} = \mathbf{G}$. We can use the property $\mathbf{G}\mathbf{v} = \mathbf{0}$ to obtain

$$E - E^- = -\frac{1}{2}(\mathbf{G}\mathbf{v}^-)^T\mathbf{D}^{-1}\mathbf{G}\mathbf{v}^-. \tag{43}$$

Since $\mathbf{D}$ is symmetric positive definite, the matrix $\mathbf{D}^{-1}$ is also symmetric positive definite so that

$$E - E^- \leq 0, \qquad \forall \mathbf{v}^-. \tag{44}$$

The choice $\mathbf{G}_\mathcal{E} = \mathbf{G}$ thus implies some dissipation of energy. This dissipation is proportional to $\mathbf{G}\mathbf{v}^-$, which is the velocity component of $\mathbf{v}^-$ orthogonal to the post-switch constraint (or the normal component of incident velocity) as illustrated in Figure 6a. This orthogonal component of $\mathbf{v}^-$ shall simply be dissipated at switching.

3.3.2 System with a single constraint

In the special case of a single constraint, we suggest the following interpolation formula:

$$\mathbf{G}_\mathcal{E} = \frac{(1-\mathcal{E})}{a^-}\mathbf{G}^- \pm \frac{\mathcal{E}}{a}\mathbf{G}, \tag{45}$$

with the normalization factors $a^- = \sqrt{\mathbf{G}^-\mathbf{M}^{-1}(\mathbf{G})^{-T}}$ and $a = \sqrt{\mathbf{G}\mathbf{M}^{-1}\mathbf{G}^T}$. The choice of the sign $\pm$ should be made according to a directional condition that will be introduced later in this section.

The energy drop $E - E^-$ in Eq. (42e) involves $\mathbf{G}_\mathcal{E}(\mathbf{v} + \mathbf{v}^-)$ which can be developed as

$$\mathbf{G}_\mathcal{E}(\mathbf{v} + \mathbf{v}^-) = \left(\frac{1-\mathcal{E}}{a^-}\right)\mathbf{G}^-\mathbf{v} \pm \frac{\mathcal{E}}{a}\mathbf{G}\mathbf{v}^-. \tag{46}$$

Since we have

$$\mathbf{v} = \mathbf{v}^- - \mathbf{M}^{-1}\mathbf{G}_\mathcal{E}^T\Lambda, \tag{47a}$$
$$= \mathbf{v}^- - \mathbf{M}^{-1}\mathbf{G}_\mathcal{E}^T\mathbf{D}_\mathcal{E}^{-1}\mathbf{G}\mathbf{v}^-, \tag{47b}$$

we obtain

$$\mathbf{G}_\mathcal{E}(\mathbf{v} + \mathbf{v}^-) = \left(-\left(\frac{1-\mathcal{E}}{a^-}\right)\mathbf{G}^-\mathbf{M}^{-1}\mathbf{G}_\mathcal{E}^T\mathbf{D}_\mathcal{E}^{-1} \pm \frac{\mathcal{E}}{a}\right)\mathbf{G}\mathbf{v}^-. \tag{48}$$

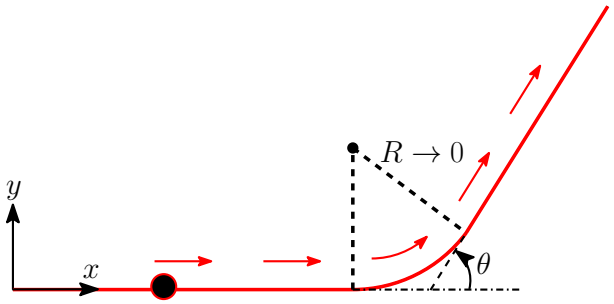

Figure 7: Point on a track such that the radius $R \to 0$.

Substituting $\mathbf{D}_\mathcal{E} = \mathbf{G}\mathbf{M}^{-1}\mathbf{G}_\mathcal{E}^T$, we obtain

$$\mathbf{G}_\mathcal{E}(\mathbf{v}+\mathbf{v}^-) = \Big(-\Big(\frac{1-\mathcal{E}}{a^-}\Big)\mathbf{G}^-\mathbf{M}^{-1}\mathbf{G}_\mathcal{E}^T(\mathbf{G}\mathbf{M}^{-1}\mathbf{G}_\mathcal{E}^T)^{-1} \pm \frac{\mathcal{E}}{a}\Big)\mathbf{G}\mathbf{v}^-. \tag{49}$$

If we consider the value $\mathcal{E} = 1/2$, i.e., if the reaction force is assumed to act in the direction of the bisector, we get

$$\mathbf{G}_{1/2}(\mathbf{v}+\mathbf{v}^-) = \frac{1}{2a}\Big(-\frac{\mathbf{G}^-\mathbf{M}^{-1}\mathbf{G}_{1/2}^T}{a^-}\Big(\frac{\mathbf{G}\mathbf{M}^{-1}\mathbf{G}_{1/2}^T}{a}\Big)^{-1} \pm 1\Big)\mathbf{G}\mathbf{v}^-, \tag{50}$$

where

$$\frac{1}{a^-}(\mathbf{G}^-\mathbf{M}^{-1}\mathbf{G}_{1/2}^T) = \frac{\mathbf{G}^-\mathbf{M}^{-1}(\mathbf{G}^-)^T}{2(a^-)^2} \pm \frac{\mathbf{G}^-\mathbf{M}^{-1}(\mathbf{G})^T}{2(a^-)a}, \tag{51a}$$

$$= \frac{1}{2} \pm \frac{\mathbf{G}^-\mathbf{M}^{-1}\mathbf{G}^T}{2a^-a}, \tag{51b}$$

$$\frac{1}{a}(\mathbf{G}\mathbf{M}^{-1}\mathbf{G}_{1/2}^T) = \frac{\mathbf{G}\mathbf{M}^{-1}\mathbf{G}^-}{2aa^-} \pm \frac{\mathbf{G}\mathbf{M}^{-1}\mathbf{G}^T}{2a^2}, \tag{52a}$$

$$= \frac{\mathbf{G}\mathbf{M}^{-1}\mathbf{G}^-}{2aa^-} \pm \frac{1}{2}, \tag{52b}$$

$$= \pm\Big(\frac{1}{a^-}\mathbf{G}^-\mathbf{M}^{-1}\mathbf{G}_{1/2}^T\Big). \tag{52c}$$

Finally, we have

$$\mathbf{G}_{1/2}(\mathbf{v}+\mathbf{v}^-) = \frac{1}{2a}(\mp 1 \pm 1)\mathbf{G}\mathbf{v}^- = 0, \tag{53}$$

which implies that $E - E^- = 0$, i.e., the energy is conserved. Thus, if the reaction force is oriented along the bisector (as illustrated in Figure 6b), the impact model results in a conservation of energy. Such a conservative model might be relevant for cases as in Figure 7, where the nonsmooth track represents the limit case of a smooth track with a radius $R \to 0$. The condition in Eq. (53) can be interpreted as an orthogonality condition between the intermediate gradient and the average velocity, which is illustrated in Figure 6b.

Let us come back to the choice of the sign in Eq. (45). We propose to define it based on a directional condition illustrated in Figure 8. We see that the post-switch gradient can either be represented by $\mathbf{G}$ or by $-\mathbf{G}$. Both vectors span the same subspace, but their choice may influence the interpolation, as $(1-\mathcal{E})\mathbf{G}^- + \mathcal{E}\mathbf{G}$ and $(1-\mathcal{E})\mathbf{G}^- - \mathcal{E}\mathbf{G}$ do not span the same subspace. We propose to fix the choice of the sign in order to ensure that,

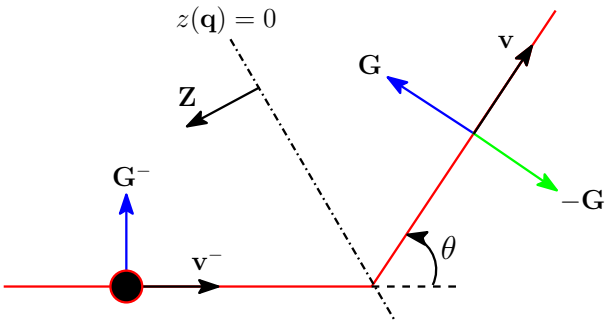

Figure 8: Directional condition.

in the case $\mathcal{E} = 1/2$, the system will cross the switching surface, and continue in the next mode with the same energy. Thus, the directional condition takes the form

$$(\mathbf{Z}\mathbf{v}^-)(\mathbf{Z}\mathbf{v}) \geq \mathbf{0}, \tag{54}$$

which can be reformulated using Eq. (47b) as

$$(\mathbf{Z}\mathbf{v}^-)(\mathbf{Z}\mathbf{v}^- - \mathbf{Z}\mathbf{M}^{-1}\mathbf{G}_{1/2}^T(\mathbf{G}\mathbf{M}^{-1}\mathbf{G}_{1/2}^T)^{-1}\mathbf{G}\mathbf{v}^-) \geq \mathbf{0}. \tag{55}$$

3.3.3 General case

In the case of a single constraint, we have already seen that the interpolation of the constraint gradient is not a trivial problem. From a geometric view point, the subspace spanned by the constraint gradient is not affected by a scaling or a change in the sign of $\mathbf{G}$. It is important that the interpolation procedure remains invariant with respect to scaling or sign changes across the switching surface. Equation (45) satisfies this requirement. The question can be generalized to problems with several constraints. However, the adaptation of the direct interpolation formula given in Eq. (29) becomes very cumbersome, as one needs to ensure invariance with respect to normalization and sign changes for the columns of $\mathbf{G}^T$ (as discussed in the previous section), but also invariance with respect to column permutations, as the column sequence might differ in $(\mathbf{G})^{-T}$ and $\mathbf{G}^T$, but these permutations do not alter the spanned subspaces. In that context, observing that the linear subspace spanned by $\mathbf{G}^T$ is an element of a Grassmann manifold [32], one may resort to interpolation methods on Grassmann manifolds [33–35] to establish a consistent interpolation procedure. However, we will not further elaborate on this question in the context of the present paper, and leave this extension as a perspective. All numerical examples treated in this paper fall in one of the special cases discussed in Sections 3.3.1 and 3.3.2.

4 Numerical time integration

The exact solution of the equations of motion should satisfy the constraints at position, velocity, and acceleration levels. Using classical DAE time integration schemes, a numerical approximation can be obtained in the smooth modes, but it may not necessarily capture the discontinuous behaviour at the switching surfaces. Methods based on smooth approximations heavily rely on the appropriate choice of a smoothing parameter, as discussed in Section 2.1, and may suffer from high numerical stiffness. They will be not be studied here. In contrast, we shall focus on methods from nonsmooth dynamics such as event-driven and time-stepping schemes.

We propose to study several possible time integration methods for this class of problems. On the one hand, the index-3 form and index-reduced forms of the classical generalized-α scheme will be considered to illustrate the behaviour and limitations of standard DAE solvers. On the other hand, event-driven and time-stepping versions of the generalized-α scheme will be analyzed in detail.

4.1 Classical DAE schemes

4.1.1 Index-3 generalized-α method

The index-3 generalized-α method can be considered to solve the index-3 DAE in Eqs. (22-24). Following the procedure described in [36], the discrete system at time step t_{n+1} is formulated as

$$\dot{\mathbf{q}}_{n+1} = \mathbf{v}_{n+1}, \tag{56}$$
$$\mathbf{M}_{n+1}\dot{\mathbf{v}}_{n+1} + \mathbf{G}_{n+1}^T\boldsymbol{\lambda}_{n+1} = \mathbf{f}_{n+1}, \tag{57}$$
$$\mathbf{g}_{n+1} = \mathbf{0}, \tag{58}$$

where we drop the functional arguments for sake of conciseness with $\mathbf{M}_{n+1} = \mathbf{M}(\mathbf{q}_{n+1})$, $\mathbf{G}_{n+1}^T = \mathbf{G}^T(\mathbf{q}_{n+1}, t_{n+1})$, $\mathbf{f}_{n+1} = \mathbf{f}(\mathbf{q}_{n+1}, \mathbf{v}_{n+1}, t_{n+1})$, and $\mathbf{g}_{n+1} = \mathbf{g}(\mathbf{q}_{n+1}, t_{n+1})$. Equations (56 - 58) are accompanied by the difference formulae

$$\mathbf{q}_{n+1} = \mathbf{q}_n + h\mathbf{v}_n + h^2(0.5-\beta)\mathbf{a}_n + h^2\beta\mathbf{a}_{n+1}, \tag{59}$$
$$\mathbf{v}_{n+1} = \mathbf{v}_n + h(1-\gamma)\mathbf{a}_n + h\gamma\mathbf{a}_{n+1}, \tag{60}$$
$$(1-\alpha_m)\mathbf{a}_{n+1} + \alpha_m\mathbf{a}_n = (1-\alpha_f)\dot{\mathbf{v}}_{n+1} + \alpha_f\dot{\mathbf{v}}_n, \tag{61}$$

where $\mathbf{a}_n$ is an auxiliary acceleration variable which is initialized as $\mathbf{a}_0 = \ddot{\mathbf{q}}_0$. The numerical parameters α_m, α_f, β, γ can be selected as

$$\alpha_m = \frac{2\rho_\infty - 1}{\rho_\infty + 1}, \qquad \alpha_f = \frac{\rho_\infty}{\rho_\infty + 1}, \tag{62}$$
$$\gamma = 0.5 + \alpha_f - \alpha_m, \qquad \beta = 0.25(\gamma + 0.5)^2, \tag{63}$$

where $\rho_\infty \in [0, 1]$ is the desired spectral radius at infinity, with $\rho_\infty = 1$ indicating no dissipation, and $\rho_\infty = 0$ meaning a complete annihilation of the high-frequency oscillations. Equations (57) and (58) are nonlinear and a Newton procedure shall be required. As explained in [36], the computation of corrections for the unknowns $\mathbf{q}_{n+1}$, $\mathbf{v}_{n+1}$, $\dot{\mathbf{v}}_{n+1}$, and $\boldsymbol{\lambda}_{n+1}$ requires an iteration matrix $\mathbf{S}_t$ which is defined as

$$\mathbf{S}_t = \begin{bmatrix} \mathbf{M}_{n+1}\beta' + \mathbf{C}_t\gamma' + \mathbf{K}_t & \mathbf{G}_{n+1}^T \\ \mathbf{G}_{n+1} & \mathbf{0} \end{bmatrix} \tag{64}$$

where $\mathbf{K}_t = \partial(\mathbf{M}_{n+1}\dot{\mathbf{v}}_{n+1} - \mathbf{f}_{n+1} + \mathbf{G}_{n+1}^T\boldsymbol{\lambda}_{n+1})/\partial\mathbf{q}_{n+1}$ is the tangent stiffness matrix and $\mathbf{C}_t = \partial(-\mathbf{f}_{n+1})/\partial\mathbf{v}_{n+1}$ is the tangent damping matrix. The parameters β' and γ' are computed as

$$\beta' = \frac{1-\alpha_m}{h^2\beta(1-\alpha_f)}, \qquad \gamma' = \frac{\gamma}{h\beta}. \tag{65}$$

Notice that in Eqs. (56-61), the velocity and acceleration level constraints are not imposed, i.e., they are hidden constraints.

4.1.2 Index-2 generalized-α method

The index-2 generalized-α formulation is obtained by substituting the constraint in Eq. (58) by its first time derivative. The dynamic equilibrium is thus solved at time t_{n+1} as

$$\dot{\mathbf{q}}_{n+1} = \mathbf{v}_{n+1}, \tag{66}$$
$$\mathbf{M}_{n+1}\dot{\mathbf{v}}_{n+1} + \mathbf{G}_{n+1}^T\boldsymbol{\lambda}_{n+1} = \mathbf{f}_{n+1}, \tag{67}$$
$$\mathbf{G}_{n+1}\mathbf{v}_{n+1} = -\mathbf{g}_{t,n+1}, \tag{68}$$

where the short notation $\mathbf{g}_{t,n+1} = \mathbf{g}_t(\mathbf{q}_{n+1}, t_{n+1})$. Equations (66 - 68) are accompanied by the difference formulae in Eqs. (59-61). The iteration matrix is not presented for the sake of conciseness, but is trivially obtained by the linearization of Eqs. (67) and (68).

A variant of this formulation which involves the intermediate gradient $\mathbf{G}_\mathcal{E}$ will also be considered in the numerical examples in Section 5. In this version, the discrete system at time step t_{n+1} is formulated as

$$\dot{\mathbf{q}}_{n+1} = \mathbf{v}_{n+1}, \tag{69}$$
$$\mathbf{M}_{n+1}\dot{\mathbf{v}}_{n+1} + \mathbf{G}^T_{\mathcal{E},n+1}\boldsymbol{\lambda}_{n+1} = \mathbf{f}_{n+1}, \tag{70}$$
$$\mathbf{G}_{n+1}\mathbf{v}_{n+1} = -\mathbf{g}_{t,n+1}, \tag{71}$$

along with the difference formulae in Eqs. (59-61). The iteration matrix can be obtained by the linearization of Eqs. (70) and (71) but is not presented for the sake of conciseness.

4.1.3 Index-1 generalized-α method

The index-1 generalized-α formulation is obtained by substituting the constraint in Eq. (58) by its second time derivative. The dynamic equilibrium is thus solved at time t_{n+1} as

$$\dot{\mathbf{q}}_{n+1} = \mathbf{v}_{n+1}, \tag{72}$$
$$\mathbf{M}_{n+1}\dot{\mathbf{v}}_{n+1} + \mathbf{G}^T_{n+1}\boldsymbol{\lambda}_{n+1} = \mathbf{f}_{n+1}, \tag{73}$$
$$\mathbf{G}_{n+1}\dot{\mathbf{v}}_{n+1} + \dot{\mathbf{G}}_{n+1}\mathbf{v}_{n+1} = -\dot{\mathbf{g}}_{t,n+1}, \tag{74}$$

along with the difference formulae in Eqs. (59-61). The iteration matrix can be obtained by the linearization of Eqs. (73) and (74).

4.2 Nonsmooth DAE schemes

4.2.1 Event-driven generalized-α method

The HDAE formulation that explicitly defines the modal transitions is best suited to be solved using event-driven schemes [26]. Such schemes are fundamentally classical DAE solvers, combined with an event-detection and a time-step adaptation strategy. This strategy can be developed based on the classical generalized-α scheme with constraints at position level in Eqs. (56-61). Switch detection procedures can rely on the switching time T_1, that is either computed analytically or using root-finding procedures. A time-step adaptation is performed so that the discrete time t_{n+1} coincides with the switching time T_1.

The integration is paused for an update of the state variables. In particular, the update of velocities $\mathbf{v}(t)$ can be done by exploiting the impact equation which involves the velocity constraint. In this way, the post-switch velocity $\mathbf{v}(t)$ is compatible with the post-switch constraint. The integration is restarted using the updated initial conditions. This update procedure ensures that $\mathbf{q}(t)$ and $\mathbf{v}(t)$ are compatible with the post-switch constraints at position and velocity levels.

4.2.2 Nonsmooth generalized-α method

Time-stepping (also known as event-capturing) schemes have been developed to obtain the solution of the equations of motion in terms of differential measures as in Eqs. (33-35). They can deal with discontinuities inside the time step, so that the time step should not be calibrated to each switching event.

In the nonsmooth generalized-α (NSGA) scheme, the position and velocity constraints are simultaneously enforced following a similar approach as proposed by Gear, Gupta, and Leimkuhler [37]. In the case of impulsive contributions, this scheme is first-order accurate. We present the decoupled version of NSGA [28] which is based on the decomposition of the position and velocity fields as

$$\mathbf{q}_{n+1} = \widetilde{\mathbf{q}}_{n+1} + \mathbf{U}_{n+1}, \tag{75}$$
$$\mathbf{v}_{n+1} = \widetilde{\mathbf{v}}_{n+1} + \mathbf{W}_{n+1}, \tag{76}$$

where $\widetilde{\mathbf{q}}_{n+1}$ and $\widetilde{\mathbf{v}}_{n+1}$ are smooth positions and velocities, and $\mathbf{U}_{n+1}$ and $\mathbf{W}_{n+1}$ are the position corrections and velocity jumps. At each time step, a sequence of three subproblems should be solved.

Firstly, the smooth motion at time step t_{n+1} is computed using the smooth constraints at velocity level $\dot{\mathbf{g}}^{\overline{\mathcal{Z}}}(\widetilde{\mathbf{q}}_{n+1}, t_{n+1}) = \mathbf{0}$ as

$$\dot{\widetilde{\mathbf{q}}}_{n+1} = \widetilde{\mathbf{v}}_{n+1}, \tag{77}$$

$$\widetilde{\mathbf{M}}_{n+1}\dot{\widetilde{\mathbf{v}}}_{n+1} + \widetilde{\mathbf{G}}_{n+1}^{\overline{\mathcal{Z}},T}\widetilde{\boldsymbol{\lambda}}_{n+1}^{\overline{\mathcal{Z}}} = \widetilde{\mathbf{f}}_{n+1}, \tag{78}$$

$$\widetilde{\mathbf{G}}_{n+1}^{\overline{\mathcal{Z}},T}\widetilde{\mathbf{v}}_{n+1} = -\widetilde{\mathbf{g}}_{t,n+1}^{\overline{\mathcal{Z}}}, \tag{79}$$

$$\widetilde{\boldsymbol{\lambda}}_{n+1}^{\mathcal{Z}} = \mathbf{0}, \tag{80}$$

where we adopt the short notation $\widetilde{\mathbf{M}}_{n+1} = \mathbf{M}(\widetilde{\mathbf{q}}_{n+1})$, $\widetilde{\mathbf{G}}_{n+1}^{\overline{\mathcal{Z}},T} = \mathbf{G}^{\overline{\mathcal{Z}},T}(\widetilde{\mathbf{q}}_{n+1}, t_{n+1})$, $\widetilde{\mathbf{f}}_{n+1} = \mathbf{f}(\widetilde{\mathbf{q}}_{n+1}, \widetilde{\mathbf{v}}_{n+1}, t_{n+1})$, and $\widetilde{\mathbf{g}}_{t,n+1}^{\overline{\mathcal{Z}}} = \mathbf{g}_t^{\overline{\mathcal{Z}}}(\widetilde{\mathbf{q}}_{n+1}, t_{n+1})$.

The variables $\widetilde{\mathbf{q}}_{n+1}$, $\widetilde{\mathbf{v}}_{n+1}$, and $\dot{\widetilde{\mathbf{v}}}_{n+1}$ should also satisfy the generalized-α integration formulae as in Eqs. (59-61). It is important to observe that the switching constraints are ignored in the definition of the smooth motion according to Eqs. (77-80). This is a fundamental difference compared to the classical index-3, index-2, and index-1 versions of the generalized-α scheme. Notice that $\widetilde{\mathbf{q}}_{n+1}$ and $\widetilde{\mathbf{v}}_{n+1}$ are decoupled from $\mathbf{U}_{n+1}$, $\mathbf{W}_{n+1}$, $\mathbf{q}_{n+1}$, and $\mathbf{v}_{n+1}$. The nonlinear system is solved for $\widetilde{\mathbf{q}}_{n+1}$, $\widetilde{\mathbf{v}}_{n+1}$, $\dot{\widetilde{\mathbf{q}}}_{n+1}$, $\widetilde{\boldsymbol{\lambda}}_{n+1}^{\overline{\mathcal{Z}}}$, and $\mathbf{a}_{n+1}$ using a Newton-Raphson technique.

Secondly, the position correction $\mathbf{U}_{n+1}$ is computed at time step t_{n+1} such that $\mathbf{q}_{n+1}$ is compatible with the set of smooth and switching bilateral constraints $\mathbf{g}(\mathbf{q}_{n+1}, t_{n+1}) = \mathbf{0}$ as

$$\dot{\mathbf{q}}_{n+1} = \mathbf{v}_{n+1}, \tag{81}$$

$$\widetilde{\mathbf{M}}_{n+1}\mathbf{U}_{n+1} + \mathbf{G}_{\mathcal{E},n+1}^{T}\boldsymbol{\nu}_{n+1} = h^2\mathbf{f}_{n+1}^{p}, \tag{82}$$

$$\mathbf{g}_{n+1} = \mathbf{0}, \tag{83}$$

where $\mathbf{f}_{n+1}^{p} = \mathbf{f}(\mathbf{q}_{n+1}, \widetilde{\mathbf{v}}_{n+1}, t_{n+1}) - \mathbf{f}(\widetilde{\mathbf{q}}_{n+1}, \widetilde{\mathbf{v}}_{n+1}, t_{n+1}) + (\mathbf{G}_{n+1}^{T}(\mathbf{q}_{n+1}, t_{n+1}) - \mathbf{G}_{n+1}^{T}(\widetilde{\mathbf{q}}_{n+1}, t_{n+1}))\widetilde{\boldsymbol{\lambda}}_{n+1}$, and $\boldsymbol{\nu}_{n+1}$ is the contribution of constraint forces to the position correction. A Newton semi-smooth method can be used to solve for $\mathbf{U}_{n+1}$, $\mathbf{q}_{n+1}$, and $\boldsymbol{\nu}_{n+1}$. In Eq. (82), $\mathbf{G}_{\mathcal{E}}$ is evaluated using a different procedure whether the time step includes the switching events or not:

$$\begin{cases} \mathbf{G}_{\mathcal{E}} = \mathbf{G} & \text{if } z_i(\mathbf{q}_n) z_i(\mathbf{q}_{n+1}) > 0, \quad \forall i, \\ \mathbf{G}_{\mathcal{E}} \text{ is defined by interpolation between } \mathbf{G}_n, \\ \text{and } \mathbf{G}_{n+1} \text{ otherwise.} \end{cases} \tag{84}$$

Thirdly, the velocity jump $\mathbf{W}_{n+1}$ is computed at time step t_{n+1} such that the velocities $\mathbf{v}_{n+1}$ satisfy the smooth velocity constraints $\dot{\mathbf{g}}^{\overline{\mathcal{Z}}}(\mathbf{q}_{n+1}, t_{n+1}) = \mathbf{0}$ as

$$\dot{\mathbf{q}}_{n+1} = \mathbf{v}_{n+1}, \tag{85}$$

$$\mathbf{M}_{n+1}\mathbf{W}_{n+1} + \mathbf{G}_{\mathcal{E},n+1}^{T}\boldsymbol{\Lambda}_{n+1} = h\mathbf{f}_{n+1}^{*}, \tag{86}$$

$$\mathbf{G}_{n+1}\mathbf{v}_{n+1} = -\mathbf{g}_{t,n+1}, \tag{87}$$

where $\mathbf{f}_{n+1}^{*} = \mathbf{f}(\mathbf{q}_{n+1}, \mathbf{v}_{n+1}, t_{n+1}) - \mathbf{f}(\widetilde{\mathbf{q}}_{n+1}, \widetilde{\mathbf{v}}_{n+1}, t_{n+1}) + (\mathbf{G}_{n+1}^{T}(\mathbf{q}_{n+1}, t_{n+1}) - \mathbf{G}_{n+1}^{T}(\widetilde{\mathbf{q}}_{n+1}, t_{n+1}))\widetilde{\boldsymbol{\lambda}}_{n+1} - (\mathbf{M}(\mathbf{q}_{n+1}) - \mathbf{M}(\widetilde{\mathbf{q}}_{n+1}))\dot{\widetilde{\mathbf{v}}}_{n+1}$. Further $\boldsymbol{\Lambda}_{n+1}$ represents the impulse of the constraint forces. In Eq. (86), $\mathbf{G}_{\mathcal{E}}$ is obtained as per the procedure in Eq. (84).

5 Numerical examples

In this section, we shall present the analysis and comparison of solutions obtained using the classical and non-smooth integration schemes of Section 4 for the benchmark test introduced in Section 2.1.1. Afterwards, the NSGA method will be used for three additional examples: a simplified braiding machine, a wheel rolling across a pothole, and a cam-follower mechanism.

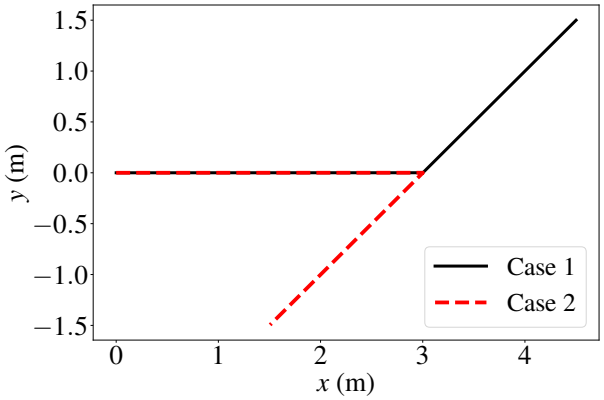

Figure 9: Material point on nonsmooth track: numerical results for the trajectory $x(t)$ and $y(t)$ for two different definitions of the switching function. Case 1: $z(\mathbf{q}) = x - l$. Case 2: $z(\mathbf{q}) = -y + \tan\theta^*/2(x - l)$ with $\theta^* = -3\pi/4$.

5.1 Material point on a nonsmooth track

Consider the benchmark problem introduced in Section 2.1.1 with $\theta = \pi/4$. Let us assume that the material point has a mass m_p. The mass matrix is thus defined as $\mathbf{M} = \text{diag}\begin{bmatrix} m_p & m_p \end{bmatrix} \in \mathbb{R}^{2\times 2}$.

In the HDAE form, the system dynamics comprises of the index-3 DAE system in the smooth modes

$$\begin{cases} \left.\begin{aligned} m_p\dot{v}_x(t) &= 0 \\ m_p\dot{v}_y(t) + \lambda &= 0 \\ y(t) &= 0 \end{aligned}\right\} & \text{if } z(\mathbf{q}(t)) < 0, \\ \left.\begin{aligned} m_p\dot{v}_x(t) - \lambda\tan(\theta) &= 0 \\ m_p\dot{v}_y(t) + \lambda &= 0 \\ y(t) - (x(t) - l)\tan(\theta) &= 0 \end{aligned}\right\} & \text{if } z(\mathbf{q}(t)) > 0. \end{cases} \tag{88}$$

along with the impact equation at the switching surface $z(\mathbf{q}) = 0$

$$\left.\begin{aligned} m_p(v_x - v_x^-) - \Lambda\tan(\theta_{\mathcal{E}}) &= 0 \\ m_p(v_y - v_y^-) + \Lambda &= 0 \\ v_y - \tan(\theta)v_x &= 0, \end{aligned}\right\} \quad \text{if } z(\mathbf{q}) = 0, \tag{89}$$

where $\theta_{\mathcal{E}}$ is the angle used to evaluate the intermediate constraint gradient $\mathbf{G}_{\mathcal{E}}$.

In this example, the number of smooth constraints is $m^{\overline{z}} = 0$ and the number of switching (nonsmooth) constraints is $m^{z} = 1$.

The physical parameters are chosen as $m_p = 1$ kg, $l = 3$ m, and $v_x = 1$ m/s. The numerical parameters for the generalized-α scheme are chosen as spectral radius $\rho_\infty = 0.98$, time step size $h = 0.002$ s, total simulation time $t_f = 6$ s, tolerance for Newton iterations as 10^{-6}, and maximum Newton iterations set to 20. The numerical parameters for the NSGA scheme are identical to the generalized-α scheme.

5.1.1 Evaluation of the energy drop

From the theoretical observations in Section 3.3.1, the choice of $\mathbf{G}_{\mathcal{E}} = \mathbf{G}$ (so here $\theta_{\mathcal{E}} = \theta$) should lead to a dissipation in energy. The energy drop can be evaluated using the expression in Eq. (43). Since the constraint gradient is $\mathbf{G}_{\mathcal{E}} = \mathbf{G} = \begin{bmatrix} -\tan(\theta) & 1 \end{bmatrix} = \begin{bmatrix} -1 & 1 \end{bmatrix}$, the Delassus operator is obtained as $\mathbf{D} = \mathbf{G}\mathbf{M}^{-1}\mathbf{G}^T = 2$. Using $\mathbf{v}^- = \begin{bmatrix} v_x & v_y \end{bmatrix}^T = \begin{bmatrix} 1 & 0 \end{bmatrix}^T$, we obtain the energy drop from Eq. (43) as

$$E - E^- = -\frac{1}{2}(\mathbf{v}^-)^T\mathbf{G}^T\mathbf{D}^{-1}\mathbf{G}\mathbf{v}^- = -0.25. \tag{90}$$

A dissipation of energy of -0.25 J is thus expected, which represents a 50% energy drop, as $E^- = 0.5$ J. In contrast, if $\mathbf{G}_{\mathcal{E}} = \mathbf{G}_{1/2}$ (so here $\theta_{\mathcal{E}} = \theta_{1/2} = (\pi + \theta)/2$), we expect that the energy is conserved.

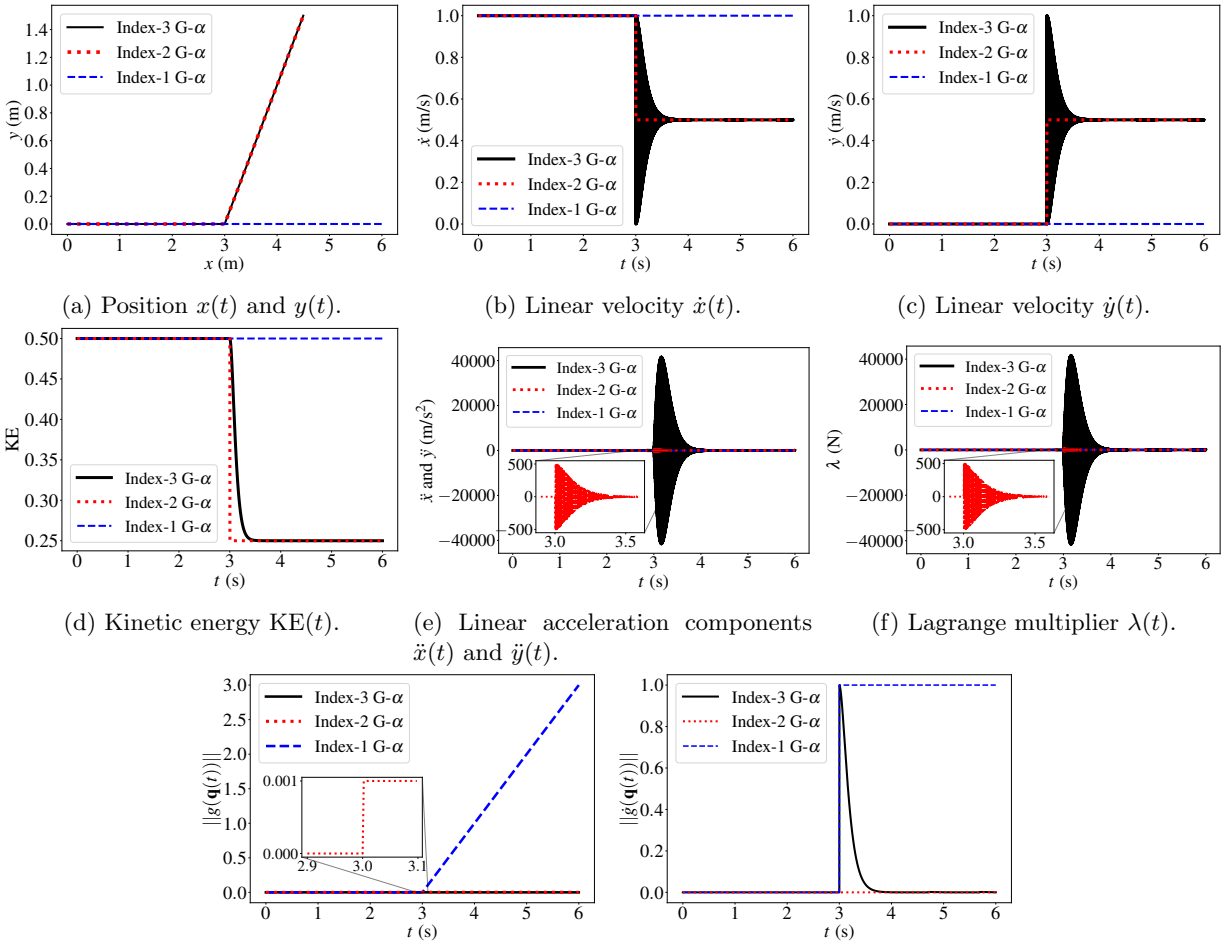

(a) Position $x(t)$ and $y(t)$.

(b) Linear velocity $\dot{x}(t)$.

(c) Linear velocity $\dot{y}(t)$.

(d) Kinetic energy KE(t).

(e) Linear acceleration components $\ddot{x}(t)$ and $\ddot{y}(t)$.

(f) Lagrange multiplier $\lambda(t)$.

(g) Residual of position constraint $||g(\mathbf{q}(t))||$.

(h) Residual of velocity constraint $||\dot{g}(\mathbf{q}(t))||$.

Figure 10: Material point on nonsmooth track for $\theta = \pi/4$ and $z(\mathbf{q}) = x - l$: comparison of numerical results obtained from classical index-3, index-2, and index-1 generalized-α methods.

5.1.2 Influence of the switching function

Let us study the influence of switching function as a follow-up of the discussion in Section 2.1. Figure 9 illustrates the numerical solution obtained using the index-2 generalized-α method for positions $x(t)$ and $y(t)$ for two choices of the switching functions. In the case 1, the solution evolves along the constraint space defined by the pre-switch constraint $y(t) = 0$ for $z(\mathbf{q}(t)) < 0$, and the post-switch constraint $y(t) = \tan(\theta)(x(t) - l)$ for $z(\mathbf{q}(t)) > 0$.

In the case 2, the solution evolves along the constraint space defined by the pre-switch constraint $y(t) = 0$ for $z(\mathbf{q}(t)) < 0$, and the post-switch constraint $y(t) = -\tan(\theta)(x(t) - l)$ for $z(\mathbf{q}(t)) > 0$. It is clearly evident that the geometry of the constraint space is controlled by the choice of switching function, as per the theoretical analysis in Section 2.1. From now, the analysis will focus on the case 1 with switching function $z(\mathbf{q}) = x - l$.

5.1.3 Comparison of results from classical and nonsmooth schemes

Let us compare the classical and nonsmooth schemes for the case $\theta_{\mathcal{E}} = \theta$.

Figure 10a illustrates the evolution of positions $\mathbf{q}(t)$, i.e., $x(t)$ and $y(t)$ of the material point across the kink. The trajectories obtained using the index-3 and index-2 methods evolve along the track. This observation is consistent with the fact that the index-3 solution satisfies the position constraint up to machine precision. The index-2 solution may not necessarily satisfy the position constraint with the same precision, as it may suffer from a constraint drift-off effect (which is later observed in Figure 10g and remains small in this case). The index-1 solution misses the kink and drifts away after the switching, and thus goes completely off the track. This demonstrates that the index-1 solution is incorrect and not acceptable. Intuitively, this behaviour can be explained because the index-1 scheme computes the position solution through the integration of the acceleration field, which remains 0 in each phase of motion. This can be confirmed from the results obtained for velocities in Figures 10b and 10c.

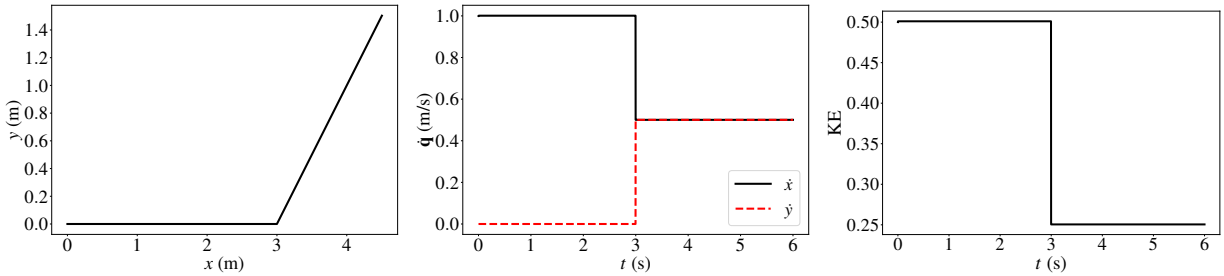

(a) Position $x(t)$ and $y(t)$.

(b) Linear velocity components $\dot{x}(t)$ and $\dot{y}(t)$.

(c) Kinetic energy KE(t).

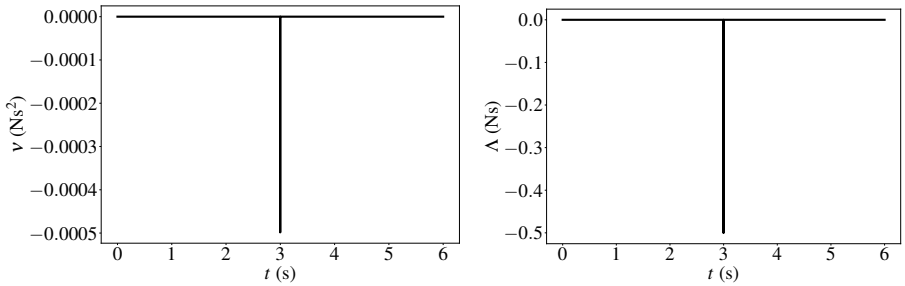

(d) Lagrange multiplier at position correction $\nu(t)$.

(e) Lagrange multiplier at velocity jump $\Lambda(t)$.

Figure 11: Material point on nonsmooth track: numerical results obtained using the NSGA method.

The evolution of velocities $\dot{x}$ and $\dot{y}$ with time are illustrated in Figures 10b and 10c respectively. Spurious oscillations of numerical origin are triggered at switching in the index-3 solution, which reflects that the numerical solution does not satisfy the hidden velocity constraints after the switching. The amplitude of the oscillations gradually decreases for $z(\mathbf{q}(t)) > 0$, thanks to the numerical damping of the generalized-α method. On the other hand, an index-2 formulation enforces the hidden velocity constraint, and results in a compatible solution for $\dot{x}$ and $\dot{y}$ as observed in Figures 10b and 10c. As expected, the index-1 method leads to constant velocities i.e., $\dot{x} = 1$ m/s and $\dot{y} = 0$ m/s for all time.

Further, the evolution of the kinetic energy (KE) with time is presented in Figure 10d. A dissipation of energy is observed at switching in the index-3 and index-2 solutions. This is in agreement with the analysis presented in Section 3.3.1. In Figure 10d, the KE drops from 0.5 J to 0.25 J, which is in agreement with the theoretical value of Eqs. (90). As the velocities obtained from the index-2 scheme are discontinuous, the decay of energy is instantaneous, whereas the decay is progressive in the index-3 solution.

Figure 10e shows the evolution of acceleration components $\ddot{x}$ and $\ddot{y}$. The index-3 and index-2 solutions, whose definition do not involve the acceleration constraints, are affected by numerical oscillations after the discontinuity. The oscillations gradually decrease due to numerical damping. On the contrary, the accelerations obtained from the index-1 scheme is $\ddot{x} = \ddot{y} = 0$. Similar observations as the accelerations are made in the evolution of the Lagrange multiplier λ in Figure 10f.

In Figure 10g, the evolution of the norm of the residual of the position level constraint $||g(\mathbf{q}(t))||$ is presented. The index-3 method satisfies the position constraint up to machine precision in this case. A numerical disturbance effect at position level of the order of 10^{-3} at the discontinuity is observed in the index-2 solution. On the contrary, for the index-1 formulation, the error increases linearly after the kink. Similarly in Figure 10h, the evolution of the norm of the residual of the velocity level constraint $||\dot{g}(\mathbf{q}(t))||$ is presented. A jump from 0 to 1 is noticed at the discontinuity in the index-3 and index-1 solutions. After the discontinuity, this residual error decays to 0 using the index-3 method, but remains at the value of 1 using the index-1 method. The residual of the velocity constraint obtained using the index-2 method reflects that, by construction, this solution exactly satisfies the velocity constraint.

Figure 11 shows the results obtained using the nonsmooth generalized-α (NSGA). Figure 11a shows that the NSGA solution evolves on the track, and satisfies the position constraints. In Figure 11b, the velocity jump at the kink can be observed, which is consistent with the fact that the numerical solution also satisfies the velocity constraints. In Figure 11c, a 50% dissipation in the kinetic energy is observed, in agreement with the theoretical value of Eq. (90). Finally, in Figures 11d and 11e, the evolution of the Lagrange multipliers for position correction ν and velocity jump Λ is presented. At the kink, an impulse is observed in ν and Λ.

From this analysis, we can conclude that the index-3 and index-1 generalized-α methods suffer either from intense numerical oscillations or from completely wrong solutions, and therefore are not well-suited to handle the discontinuities induced at switching. We thus exclude them from further analysis. On the contrary, the

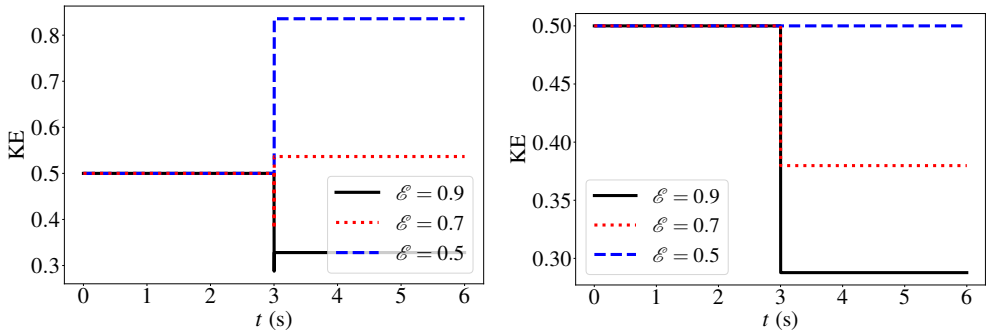

(a) Influence of $\mathcal{E}$ on the kinetic energy KE(t): index-2 generalized-α method.

(b) Influence of $\mathcal{E}$ on the kinetic energy KE(t): index-2 fully-implicit method.

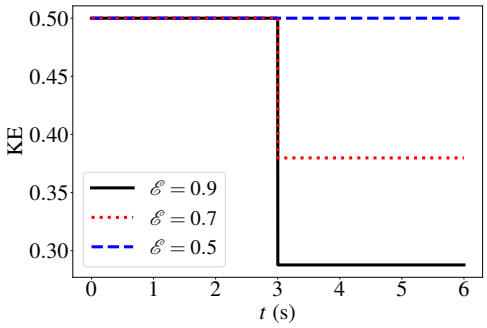

(c) Influence of $\mathcal{E}$ on the kinetic energy KE(t): NSGA and event-driven generalized-α method.

Figure 12: Kinetic energy (KE) for different values of the interpolation parameter $\mathcal{E}$.

index-2 generalized-α method provides acceptable solutions for the positions and velocities. The NSGA method provides accurate solutions, and is robust in handling the switch-induced discontinuities. For this example, the results obtained using the event-driven generalized-α scheme, are in agreement with the NSGA solution. Thus, we continue our analysis only for the index-2 generalized-α and the nonsmooth schemes.

5.1.4 Effect of gradient interpolation on energy behaviour at switching

In this section, we choose the gradient at impact $\mathbf{G}_\mathcal{E}$ as an intermediate value between $\mathbf{G}^-$ and $\mathbf{G}$ according to Eq. (45). In particular, for $\mathcal{E} = 1/2$, the gradient $\mathbf{G}_\mathcal{E}$ coincides with the bisector and we expect a conservation of energy. The extreme case $\mathcal{E} = 1$ coincides with the choice $\mathbf{G}_\mathcal{E} = \mathbf{G}$, which was studied in the previous section.

Figure 12a represents the energy using the variant of the index-2 generalized-α method which involves the intermediate gradient $\mathbf{G}_\mathcal{E}$. For $\mathcal{E} = 0.9$, we observe an energy loss at the kink, while the values $\mathcal{E} = 0.7$ and 0.5 result in an increase in energy. This is clearly an unacceptable numerical artifact of the index-2 generalized-α scheme.

This behaviour can be avoided by considering a purely implicit scheme with the values of $\gamma = 1$, $\alpha_m = 0$, $\alpha_f = 0$, and $\beta = 0.5$ in the index-2 integration procedure. The integration formulae become

$$\mathbf{q}_{n+1} = \mathbf{q}_n + h\mathbf{v}_n + \frac{h^2}{2}\mathbf{a}_{n+1}, \tag{91}$$

$$\mathbf{v}_{n+1} = \mathbf{v}_n + h\mathbf{a}_{n+1}, \tag{92}$$

$$\mathbf{a}_{n+1} = \dot{\mathbf{v}}_{n+1}, \tag{93}$$

with the special property that they do not involve the preceding accelerations in $\dot{\mathbf{v}}_n$ and $\mathbf{a}_n$ anymore. This property is favourable in handling instantaneous changes in dynamical regimes. Figure 12b represents the results obtained using this fully implicit integration. Figure 12b shows that consistent results are then obtained, and that a conservation of energy can indeed be achieved for $\mathcal{E} = 0.5$. From these results, we can say that the classical index-2 generalized-α method is generally not applicable to systems with switching bilateral constraints, unless very specific and non-optimal coefficients are selected. Actually the choice $\alpha_m = 0$, $\alpha_f = 0$, $\gamma = 1$, $\beta = 0.5$ is known to induce very high levels of numerical dissipation, and is only first order accurate even for smooth ODEs and DAEs.

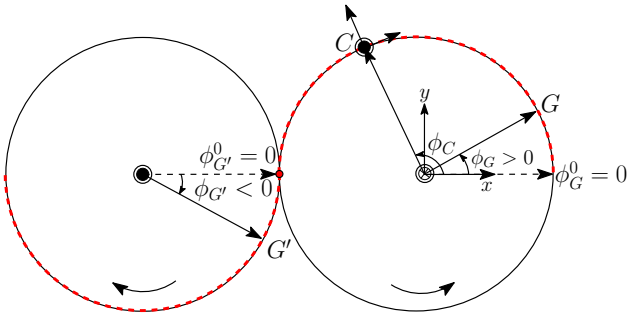

Figure 13: Multibody model of a braiding machine.

Notice that the energy behaviour as illustrated in Figure 12b can also be obtained by introducing an explicit computation of the velocity jump at $z(\mathbf{q}) = 0$ in the index-2 algorithm, in the spirit of an event-driven strategy. This can be done by explicitly introducing the impact equation that is presented in Eqs. (31-32) in the index-2 algorithm, leading to an event-driven generalized-α scheme. Thus, we can state that the event-driven generalized-α scheme leads to an energetically acceptable numerical solution.

The NSGA procedure naturally incorporates the impact model in a robust manner. Figure 12c shows that the numerical solution satisfies the conservation of energy for $\mathcal{E} = 0.5$. Therefore, we can conclude that the NSGA method stands out as a suitable integration method, which is able to handle the nonsmooth dynamics of switching bilateral constraints in an efficient and robust manner. The next examples shall therefore be solely treated using the NSGA method.

5.2 Multibody modelling of a braiding machine

In this section, we consider a slightly more complex example of a multibody system with both smooth and switching bilateral constraints.

Let us consider a simplified braiding machine with a bobbin carrier C of mass m_C (which includes the mass of textile yarn), radius r_C, and inertia j_C about its axis of rotation. The carrier interacts with two opposite rotating horn gears G and G' as shown in Figure 13 to produce the desired motions in a braiding process. Let us assume that the gear G is controlled by the motor and is thus the driving gear. Horn gears G and G' have masses m_G and $m_{G'}$ (we assume $m_G = m_{G'}$), radii r_G and $r_{G'}$, and inertia j_G and $j_{G'}$ about their respective axes of rotations. We assume that the centers of horn gears G and G' are fixed at $\begin{bmatrix} x_G & y_G \end{bmatrix}$ and $\begin{bmatrix} x_{G'} & y_{G'} \end{bmatrix}$ respectively with $x_G = y_G = y_{G'} = 0$ and $x_{G'} = -r_G - r_{G'}$.

Let $\mathbf{q}(t) = \begin{bmatrix} x_C(t) & y_C(t) & \phi_C(t) & \phi_G(t) & \phi_{G'}(t) \end{bmatrix}^T \in \mathbb{R}^5$ describe the configuration of the 1 DoF system, where $\begin{bmatrix} x_C(t) & y_C(t) \end{bmatrix}^T$ is the position of the carrier, and $\begin{bmatrix} \phi_C(t) & \phi_G(t) & \phi_{G'}(t) \end{bmatrix}^T$ are the angles defining the orientation of these three bodies. Thus we introduce 4 algebraic constraints $\mathbf{g}(\mathbf{q}(t)) = \mathbf{0}_{4\times 1}$. The initial condition on the horn gears for $t = 0$ are defined as $\phi_G(0) = 0, \phi_{G'}(0) = 0$. The initial conditions on the carrier for $t = 0$ is defined as $\phi_C(0) = \phi_G(0) + \phi_{GC}$ where ϕ_{GC} is a fixed angle between the gear G and carrier C. The position of the carrier C is initialized as $x_C(0) = r_G \cos(\phi_C(0))$, and $y_C(0) = r_G \sin(\phi_C(0))$. An initial velocity for $t = 0$ is introduced for the driving gear G as $\dot{\phi}_G(0) = \omega_G$. Consistent values of initial velocities are introduced for the carrier and gear G' as $\dot{\phi}_C(0) = \omega_G$, and $\dot{\phi}_{G'}(0) = -\omega_G$, $\dot{x}_C(0) = 0$, and $\dot{y}_C(0) = \omega_G r \cos(\phi_C)$.

Initially, the carrier is constrained to horn gear G, which defines the mode 1. The following bilateral constraint is satisfied for $z(\mathbf{q}(t)) < 0$

$$\mathbf{g}_1^{\mathcal{Z}}(\mathbf{q}(t)) = \begin{bmatrix} x_C(t) - x_G - r_G \cos(\phi_C(t)) \\ y_C(t) - y_G - r_G \sin(\phi_C(t)) \\ \phi_C(t) - \phi_G(t) - \phi_{GC} \end{bmatrix} = \mathbf{0}_{3\times 1}, \tag{94}$$

The switching function is selected as $z(\mathbf{q}) = \phi_G - \pi$. At $z(\mathbf{q}) = 0$, as the carrier is transferred to horn gear G' which defines the mode 2, the expression of the bilateral constraint instantaneously changes. The following bilateral constraint is satisfied for $z(\mathbf{q}(t)) > 0$

$$\mathbf{g}_2^{\mathcal{Z}}(\mathbf{q}(t)) = \begin{bmatrix} x_C(t) - x_{G'} + r_{G'} \cos(\phi_C(t)) \\ y_C(t) - y_{G'} + r_{G'} \sin(\phi_C(t)) \\ \phi_C(t) - \phi_{G'}(t) - \phi_{G'C} \end{bmatrix} = \mathbf{0}_{3\times 1}, \tag{95}$$

where, $\phi_{G'C}$ is the fixed angle between gear G' and carrier C.

At the switching surface $z(\mathbf{q}) = 0$, the impact model involves the intermediate gradient which is chosen as $\mathbf{G}_{\mathcal{E}} = \mathbf{G}$. From this choice, a dissipation of energy is expected at carrier transfer. At switching, a continuity requirement at position level is introduced for a smooth transfer of the carrier. From Eqs. (94) and (95), the condition of intersection of the two portions of the constraint space can be formulated as

$$\phi_G(t) + \phi_{GC} = \phi_{G'}(t) + \phi_{G'C}, \tag{96}$$

which should be fulfilled for $z(\mathbf{q}) = 0$, i.e., $\phi_G(t) = \pi$ and $\phi_{G'}(t) = -\pi$, so that we get the condition $\phi_{G'C} = \phi_{GC} + 2\pi$.

Notice that in addition to the switching constraints $\mathbf{g}^{\mathcal{Z}}(\mathbf{q}(t))$, a smooth constraint $\mathbf{g}^{\overline{\mathcal{Z}}}(\mathbf{q}(t))$ represents the coupling of the rotation of the two horn gears as

$$\mathbf{g}^{\overline{\mathcal{Z}}}(\mathbf{q}(t)) = \left[\phi_G(t) + \phi_{G'}(t)\right] = 0_{1\times 1}, \tag{97}$$

In this example, the number of smooth constraints is $m^{\overline{\mathcal{Z}}} = 1$ and the number of switching (nonsmooth) constraints is $m^{\mathcal{Z}} = 3$. The inertia matrix is defined as $\mathbf{M} = \text{diag}\begin{bmatrix} m_C & m_C & j_C & j_G & j_{G'} \end{bmatrix} \in \mathbb{R}^{5\times 5}$, where the inertia of the carrier is defined as $j_C = 1/2 m_C r_C^2$, and the inertia of the horn gears G and G' is $j_G = 1/2 m_G r_G^2$ and $j_{G'} = 1/2 m_{G'} r_{G'}^2$, respectively.

5.2.1 Results and discussions

The physical parameters are chosen as $m_C = 2$ kg, $r_C = 0.5$ m, $m_G = m_{G'} = 15$ kg. Let us assume that $r_G = 2$ m. We shall present two cases for $r_{G'} = r_G$ and $r_{G'} = 0.5 r_G$. The fixed angle between gear G and carrier C is $\phi_{GC} = 0$. The initial angular velocity of the horn gear G is $\omega_G = 1.6$ rad/s. The total simulation time is $t_f = 4$ s and $h = 0.001$ s. The numerical parameters for the NSGA scheme are chosen as in Section 5.1.

Figure 14 represents the results obtained using the NSGA scheme for carrier switching between equiradial horn gears ($r_G = r_{G'}$). In Figure 14a, the position coordinates $x_C(t)$ and $y_C(t)$ appear to be continuous everywhere, so that the transfer of carrier between horn gears seems rather smooth. In Figure 14b, a kink is observed in the evolution of $\phi_C(t)$. Such a nonsmooth behaviour reflects the discontinuity of the angular velocity $\dot{\phi}_C(t)$ at the transfer. Similarly, the angular evolution of horn gears gears $\phi_G(t)$ and $\phi_{G'}(t)$ is continuous but not necessarily differentiable, as a small velocity jump occurs in the evolution of horn gears at the transfer point.

In Figure 14d, a jump is noticed for $\dot{\phi}_C(t)$. Similar velocity jumps of small amplitude (that are barely visible in the plots) are present in the evolution of $\dot{\phi}_G(t)$ and $\dot{\phi}_{G'}(t)$. Furthermore, the behaviour of the tangential and normal components of linear velocity, i.e., $\dot{x}_C(t)$ and $\dot{y}_C(t)$ across the switching surface, along with its norm $||\dot{x}_C^2(t) + \dot{y}_C^2(t)||$ are shown in Figure 14c. If the equiradial horn gears rotate with constant angular velocities, the linear velocities should be smooth and continuous. However, this is not necessarily true, as the impulsive switching behaviour contaminates the system dynamics. Therefore jumps of small magnitude (that are barely visible in the plots) are present in the linear velocities.

Figure 14e shows the evolution of the kinetic energy (KE) with time. As expected, a dissipation of energy is observed at switching, as the intermediate gradient is chosen to be the post-switch gradient. The evolution of Lagrange multipliers for position correction $\boldsymbol{\nu}(t)$ and velocity jump $\boldsymbol{\Lambda}(t)$ is presented in Figures 14f and 14g. As the constraint expressions instantaneously switch, an impulse is observed in the constraint forces. The smooth Lagrange multiplier involved in the smooth problem $\widetilde{\lambda}^{\overline{\mathcal{Z}}}(t) = 0$.

Let us also analyze the case a carrier switching between horn gears of radii $r_{G'} = 0.5 r_G$, which nevertheless rotate with the same angular velocity $\dot{\phi}_{G'} = -\dot{\phi}_G$. Figure 15a shows that the trajectory of carrier $x_C(t)$ and $y_C(t)$ is continuous. Next, Figure 15b illustrates the evolution of linear velocities $\dot{x}_C(t)$, $\dot{y}_C(t)$, along with its norm $||\dot{x}_C^2(t) + \dot{y}_C^2(t)||$. A large jump is noticed in the tangential component of velocity $\dot{y}_C(t)$ at the transfer. Indeed the tangential velocity of the carrier $\dot{y}_C$ jumps from $\dot{y}_C = -r_G \dot{\phi}_G$ to $\dot{y}_C = 2 r_G \dot{\phi}_{G'}$ with $\dot{\phi}_{G'} = -\dot{\phi}_G$. Finally, a dissipation of energy at $z(\mathbf{q}) = 0$ is noticed in Figure 15c.

5.3 Wheel rolling across a pothole

In this section, we analyze a planar mechanical system whose dynamics is punctuated by multiple switching surfaces.

Consider a wheel of radius r, having mass m, and inertia j about its axis of rotation. In this model, we assume that the wheel remains always in closed contact with the ground, and that it rolls without slipping. The ground has, however, a nonsmooth geometry with a pothole as shown in Figure 16a. When the wheel enters the pothole, we assume that it remains in non-slipping contact with the upper left corner until it enters in contact with the upper right corner. Then, the wheel continues the motion to leave the pothole, and finally rolls without slipping along the right portion of the ground.

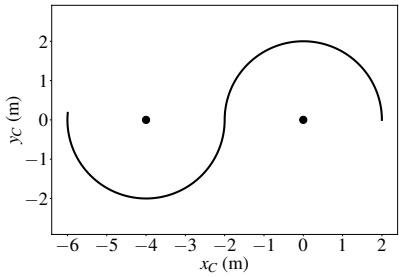

(a) Carrier trajectory $x_C(t)$ and $y_C(t)$.

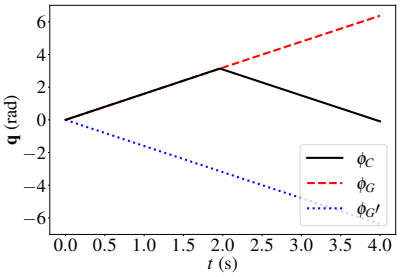

(b) Angular coordinates $\phi_C(t)$, $\phi_G(t)$, and $\phi_{G'}(t)$.

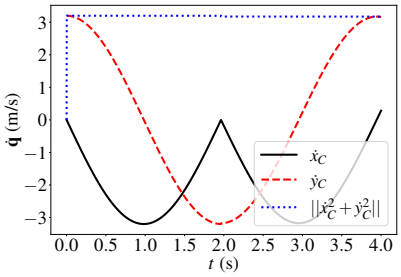

(c) Tangential and normal velocities $\dot{x}_C(t)$ and $\dot{y}_C(t)$.

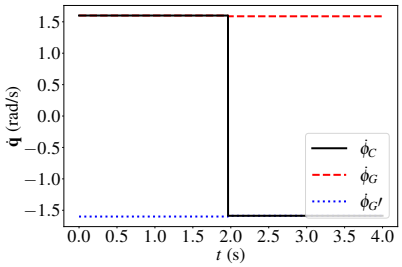

(d) Angular velocities $\dot{\phi}_C(t)$, $\dot{\phi}_G(t)$, and $\dot{\phi}_{G'}(t)$.

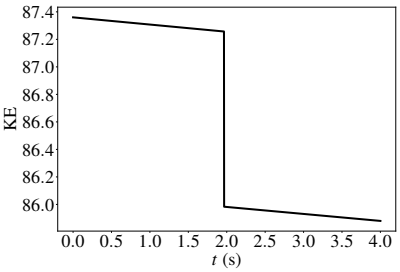

(e) Kinetic energy KE(t).

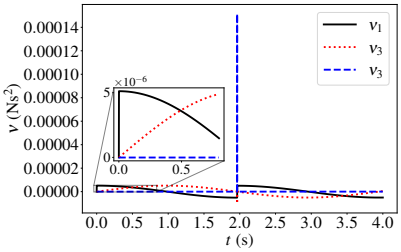

(f) Lagrange multiplier for the position correction $\boldsymbol{\nu}(t)$.

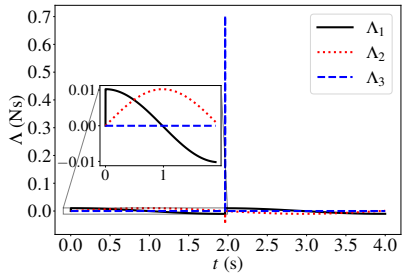

(g) Lagrange multiplier for the velocity jump $\boldsymbol{\Lambda}(t)$.

Figure 14: Numerical results for multibody model of a braiding machine having horn gear radii $r_G = r_{G'}$.

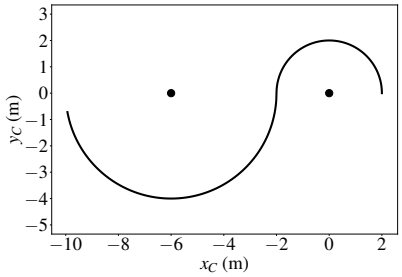

(a) Carrier trajectory $x_C(t)$ and $y_C(t)$.

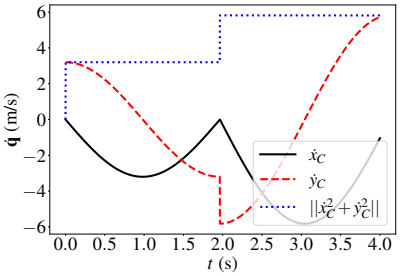

(b) Linear velocity of carrier $\dot{x}_C$ and $\dot{y}_C$.

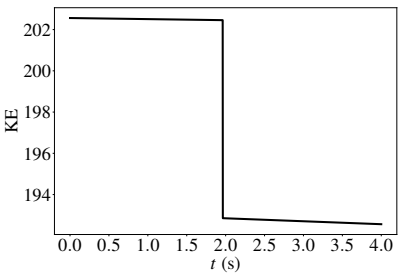

(c) Kinetic energy KE(t).

Figure 15: Numerical results for multibody model of a braiding machine having horn gear radii $r_{G'} = 0.5r_G$.

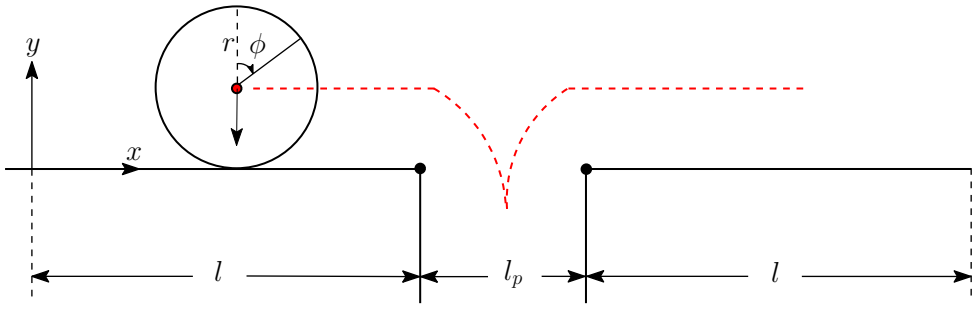

(a) Wheel rolling across a pothole.

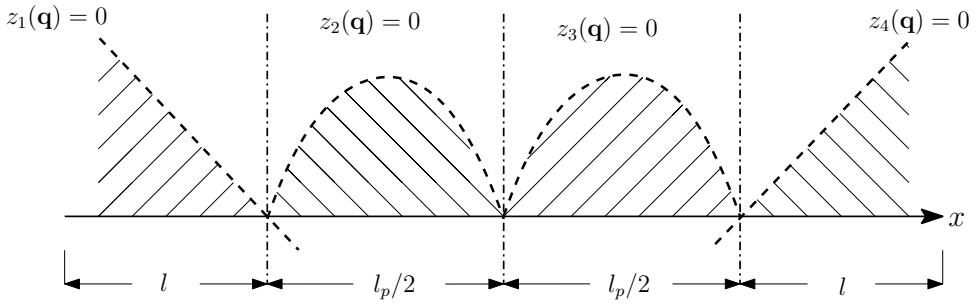

(b) Illustration of two linear switching surfaces $z_1(\mathbf{q}) = 0$ and $z_4(\mathbf{q}) = 0$, and two quadratic switching surfaces $z_2(\mathbf{q}) = 0$ and $z_3(\mathbf{q}) = 0$.

Figure 16: Illustration of the model for wheel rolling across a pothole and definition of switching surfaces.

Let us describe the 1-DoF system using a set of 3 coordinates $\mathbf{q}(t) = \begin{bmatrix} x(t) & y(t) & \phi(t) \end{bmatrix}^T \in \mathbb{R}^{3\times 1}$, which satisfy 2 algebraic constraints $\mathbf{g}(\mathbf{q}(t)) = \mathbf{0}_{2\times 1}$. The initial conditions of the wheel are defined for $t = 0$ as $x(0) = 0, y(0) = r, \phi(0) = 0$. Consistent initial velocities for $t = 0$ are introduced as $\dot{x}(0) = v_x$, $\dot{y}(0) = 0$, and $\dot{\phi}(0) = v_x/r$. The gravitational force is taken into account in this example. It should be noted that v_x should be sufficiently small to avoid loss of contact between the wheel and the ground.

The wheel is initially rolling without slipping and constrained to a horizontal track of length l (mode 1). At $x(t) = l$, the rolling wheel starts rotating about a pivot point, as it falls under gravity into the pothole of length $l_p \leq r$ (mode 2). Instantaneously at $x(t) = (l + l_p)/2$, the pivot point switches to $x(t) = l + l_p$ (mode 3). The final phase of motion $x(t) > l + l_p$ is defined by the wheel rolling on a horizontal track (mode 4). The system dynamics is thus punctuated into 4 modes defined by 4 switching functions as

$$\mathbf{z}(\mathbf{q}) = \begin{bmatrix} z_1(\mathbf{q}) & z_2(\mathbf{q}) & z_3(\mathbf{q}) & z_4(\mathbf{q}) \end{bmatrix}. \tag{98}$$

Referring to Figure 16b, the switching functions are defined as

$$z_1(\mathbf{q}) = -x + l, \tag{99}$$
$$z_2(\mathbf{q}) = -(x - l)(x - l - l_p/2), \tag{100}$$
$$z_3(\mathbf{q}) = -(x - l - l_p/2)(x - l - l_p), \tag{101}$$
$$z_4(\mathbf{q}) = x - l - l_p. \tag{102}$$

In this case, they only depend on the coordinate x, and not on y and ϕ. Notice that $z_1(\mathbf{q}) = 0$ and $z_4(\mathbf{q}) = 0$ are linear surfaces, while $z_2(\mathbf{q}) = 0$ and $z_3(\mathbf{q}) = 0$ are quadratic switching surfaces.

Let us develop the bilateral constraint expressions for each mode. The constraint expression for mode 1 is formulated as

$$\mathbf{g}_1^{\mathcal{Z}}(\mathbf{q}(t)) = \begin{bmatrix} x(t) - r\phi(t) \\ y(t) - r \end{bmatrix} = \mathbf{0}_{2\times 1} \qquad \text{if } z_1(\mathbf{q}(t)) > 0. \tag{103}$$

The condition $z_1(\mathbf{q}) = 0$ is reached when $x = l$ which implies, using Eq. (103), that $\phi = \phi^* = l/r$. In this phase, the angle thus evolves in the range $\phi(t) \in [0, \phi^*[$.

In mode 2, the constraint equations are reformulated for the wheel pivoting about the point to $x = l$, $y = 0$. The following bilateral constraint is satisfied for $z_2(\mathbf{q}(t)) > 0$

$$\mathbf{g}_2^{\mathcal{Z}}(\mathbf{q}(t)) = \begin{bmatrix} x(t) - l - r\sin(\phi(t) - \phi^*) \\ y(t) - r\cos(\phi(t) - \phi^*) \end{bmatrix} = \mathbf{0}_{2\times 1}, \tag{104}$$

The condition $z_2(\mathbf{q}) = 0$ is reached both when $x = l$ (and $\phi = \phi^*$) and when $x = l + l_p/2$. In the second case, using Eq. (104), the angle $\phi = \phi^{**}$ is such that

$$l + l_p/2 = l + r\sin(\phi^{**} - \phi^*), \tag{105}$$

so that

$$\phi^{**} = \arcsin\left(\frac{l_p}{2r}\right) + \phi^*. \tag{106}$$

In this phase, the angle evolves in the range $\phi(t) \in]\phi^*, \phi^{**}[$.

In mode 3, the angle evolves in the interval $\phi(t) \in]\phi^{**}, \phi^{***}[$. A symmetry condition between phase 2 and 3 implies that $\phi^{**} - \phi^* = \phi^{***} - \phi^{**}$, which is used to compute the expression of ϕ^{***} as

$$\phi^{***} = 2\arcsin\left(\frac{l_p}{2r}\right) + \phi^*. \tag{107}$$

Then in mode 3, the following bilateral constraint is satisfied for $z_3(\mathbf{q}(t)) > 0$

$$\mathbf{g}_3^{\mathcal{Z}}(\mathbf{q}(t)) = \begin{bmatrix} x(t) - l - l_p - r\sin(\phi(t) - \phi^{***}) \\ y(t) - r\cos(\phi(t) - \phi^{***}) \end{bmatrix} = \mathbf{0}_{2\times 1}, \tag{108}$$

where $\phi^{**} < \phi(t) < \phi^{***}$. Finally in mode 4, the bilateral constraint is similar to mode 1 and is satisfied for $z_4(\mathbf{q}(t)) > 0$

$$\mathbf{g}_4^{\mathcal{Z}}(\mathbf{q}(t)) = \begin{bmatrix} x(t) - l - l_p - r(\phi(t) - \phi^{***}) \\ y(t) - r \end{bmatrix} = \mathbf{0}_{2\times 1}. \tag{109}$$

At the switching surfaces, the impact model is defined using the post-switch gradient as $\mathbf{G}_{\mathcal{E}} = \mathbf{G}$, and thus a dissipation of energy is expected.

The inertia matrix is defined as $\mathbf{M} = \text{diag}\,[m, m, j] \in \mathbb{R}^{3\times 3}$ where $j = 1/2mr^2$. The external force vector includes the gravitational forces as $\mathbf{f}^{\text{ext}} = \begin{bmatrix} 0 & -mg & 0 \end{bmatrix}^T$, which contributes to the potential energy of the system as $\mathcal{V}(\mathbf{q}(t)) = -\mathbf{q}(t)^T\mathbf{f}^{\text{ext}}$.

In this example, the number of smooth constraints is $m^{\overline{\mathcal{Z}}} = 0$ and the number of switching (nonsmooth) constraints is $m^{\mathcal{Z}} = 2$.

5.3.1 Results and discussions

The physical parameters are defined as $m = 5$ kg, $r = 1.5$ m, $l = 2$ m, $l_p = 1$ m, $g = 9.81$ m/s^2, and $v_x(0) = 1.4$ m/s. The total simulation time is $t_f = 4$ s and $h = 0.001$ s. The numerical parameters for the NSGA scheme are chosen as in Section 5.1.

Figure 17a shows the trajectory of the wheel $x(t)$ and $y(t)$. At $x(t) = l + l_p/2$, i.e., at the switching between modes 2 and 3, a kink is observed, which indicates the presence of a discontinuity at velocity level. Figure 17b illustrates the evolution of linear velocities $\dot{x}$ and $\dot{y}$, and angular velocity $\dot{\phi}$. A strong discontinuity in the evolution of $\dot{y}(t)$ is noticed also at the bottom of the hole, i.e., at the switching between modes 2 and 3. In Figures 17c and 17d, the evolution of the Lagrange multipliers $\boldsymbol{\nu}$ and $\boldsymbol{\Lambda}$ exhibit impulsive behaviours at switching. Finally, in Figure 17e, we observe that some energy is dissipated at the transition of modes 2 and 3.

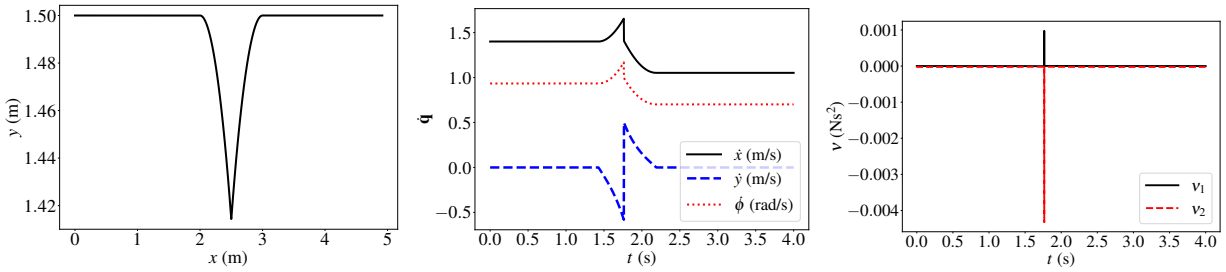

(a) Wheel trajectory $x(t)$ and $y(t)$. (b) Linear velocities $\dot{x}(t)$, $\dot{y}(t)$, and angular velocity $\dot{\phi}(t)$. (c) Lagrange multiplier for the position correction $\boldsymbol{\nu}(t)$.

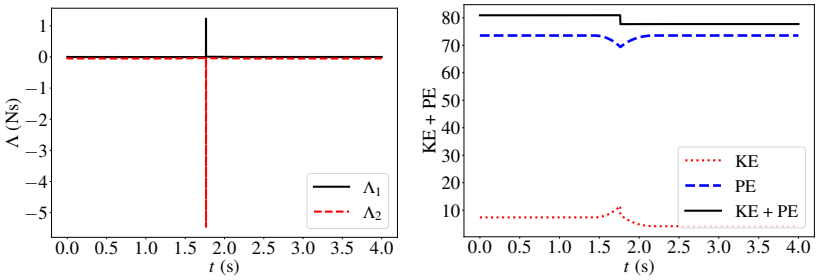

(d) Lagrange multiplier for the velocity jump $\boldsymbol{\Lambda}(t)$. (e) Total energy (KE + PE).

Figure 17: Numerical results for wheel across pothole with 4 switching surfaces.

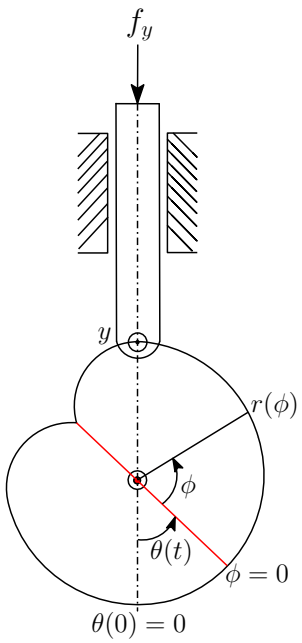

Figure 18: Cam and follower mechanism.

5.4 Cam and follower mechanism

Finally, we study a planar mechanical system in which the switching surfaces are defined periodically.

Consider a cam and follower mechanism where the cam rotates about a fixed axis, which produces a reciprocating translational motion of the follower. Let m be the mass of the cam and j be the inertia about the camshaft. Let us describe the system using coordinates $\mathbf{q}(t) = \begin{bmatrix} y(t) & \theta(t) \end{bmatrix}^T$, where $\theta(t)$ is the cam rotation, and $y(t)$ represents the linear motion of the follower. We choose polar coordinates $\begin{bmatrix} \phi(\theta(t)) & r(\phi(t)) \end{bmatrix}^T$ in the cam-attached frame to define the cam geometry as shown in Figure 18. The geometry can be defined by a periodic function $r(\phi)$.

The motion of the follower is determined by the radial coordinate $r(t)$ at the upper point of the cam, i.e., the point at polar angle $\phi(t)$ such that $\phi(t) + \theta(t) = \pi$. In the interval $\phi \in]-\pi, \pi[$, (i.e., $\theta \in]0, 2\pi[$), we choose $r(\phi) = r_0 + a\cos(\phi/2)$, where r_0 and a are constant. Out of this interval, the radius pattern is repeated periodically. The initial conditions are defined for the cam as $\theta(0) = 0$ and $\phi(0) = \pi - \theta(0) = \pi$, $r(0) = r_0 + a\cos(\phi(0)/2)$. The initial conditions of the follower are $y(0) = r(0)$. A consistent initial velocity is introduced for the cam as $\dot{\theta}(0) = \omega$ and $\dot{y}(t) = r\dot{\theta}(t)$. A downward external force f_y also acts on the follower.

The algebraic expression of the switching constraints $\mathbf{g}^{\mathcal{Z}}(\mathbf{q}(t))$ can be based on the functions

$$\begin{cases} & \vdots \\ \mathbf{g}_1^{\mathcal{Z}}(\mathbf{q}(t)) & = y(t) - r_0 - a\cos\left(\dfrac{\theta(t)}{2} + \dfrac{\pi}{2}\right), \\ \mathbf{g}_2^{\mathcal{Z}}(\mathbf{q}(t)) & = y(t) - r_0 - a\cos\left(\dfrac{\theta(t)}{2} - \dfrac{\pi}{2}\right), \\ \mathbf{g}_3^{\mathcal{Z}}(\mathbf{q}(t)) & = y(t) - r_0 - a\cos\left(\dfrac{\theta(t)}{2} - \dfrac{3\pi}{2}\right), \\ & \vdots \end{cases} \tag{110}$$

and defined in periodic form as

$$\mathbf{g}^{\mathcal{Z}}(\mathbf{q}(t)) = \begin{cases} & \vdots & \\ \mathbf{g}_1^{\mathcal{Z}}(\mathbf{q}(t)) & & \text{if } -2\pi < \theta(t) < 0, \\ \mathbf{g}_2^{\mathcal{Z}}(\mathbf{q}(t)) & & \text{if } 0 < \theta(t) < 2\pi, \\ \mathbf{g}_3^{\mathcal{Z}}(\mathbf{q}(t)) & & \text{if } 2\pi < \theta(t) < 4\pi. \\ & \vdots & \end{cases} \tag{111}$$

Alternatively, the nonsmooth evolution across $z(\mathbf{q}) = 0$ can be defined by the modulo operator denoted by %, which shall normalize the evolution of $\theta(t)$ between $[0, 2\pi]$. The generalized constraint is thus represented as

$$\mathbf{g}^{\mathcal{Z}}(\mathbf{q}(t)) = y(t) - r_0 - a\cos\left(\frac{(\theta \,\%\, 2\pi) - \pi}{2}\right), \tag{112}$$

and the switching surfaces are defined by the condition $\theta = 2p\pi$ with $p \in \mathbb{Z}$. The impact model at the switching surfaces is defined using the post-switch constraint $\mathbf{G}_{\mathcal{E}} = \mathbf{G}$, which indicates that a dissipation of energy is expected.

The inertia matrix is defined as $\mathbf{M} = \text{diag}\begin{bmatrix} m & j \end{bmatrix} \in \mathbb{R}^{2\times 2}$. The potential energy $\mathcal{V}(\mathbf{q}(t)) = -\mathbf{q}(t)^T\mathbf{f}^{\text{ext}}$ shall include the contribution of the applied force f_y as $\mathbf{f}^{\text{ext}} = \begin{bmatrix} -f_y & 0 \end{bmatrix}^T$.

In this example, the number of smooth constraints is $m^{\overline{\mathcal{Z}}} = 0$ and the number of switching (nonsmooth) constraints is $m^{\mathcal{Z}} = 1$.

5.4.1 Results and discussions

The physical parameters are chosen as $m = 1$ kg, $r_0 = 2$, $a = 1$, $\theta = 0$ rad, $\omega = 4$ rad/s, $f_y = -5$ N. The total simulation time is $t_f = 4$ s and $h = 0.001$ s. The numerical parameters for the NSGA scheme are chosen as in Section 5.1.

Figure 19a illustrates the evolution of the linear coordinate of the follower $y(t)$ with respect to the angular coordinate of the cam $\theta(t)$. Kinks are present at the switching angles 0 and 2π, which indicate the presence of

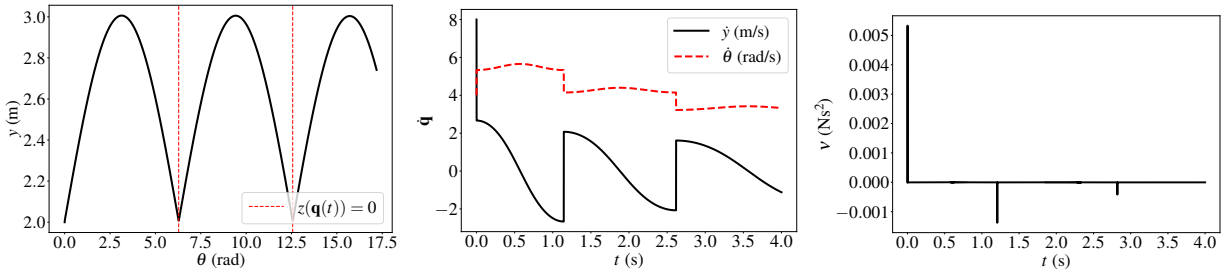

(a) Linear coordinate of follower $y(t)$ with angle $\theta(t)$ of cam.

(b) Linear velocity of follower $\dot{y}(t)$ and angular velocity of cam $\dot{\theta}(t)$.

(c) Lagrange multiplier for the position correction $\nu(t)$.

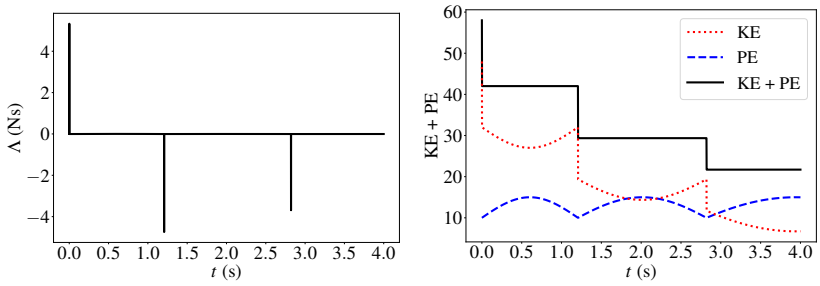

(d) Lagrange multiplier for the velocity jump $\Lambda(t)$.

(e) Total energy (KE + PE).

Figure 19: Numerical results for cam and follower mechanism.

discontinuities at velocity level. This can be confirmed in Figure 19b, which represents the evolution of linear and angular velocities.

Furthermore, Figures 19c and 19d illustrate impulsive contributions in the Lagrange multipliers ν and Λ. Finally, the evolution of kinetic (KE), potential (PE), and total energy (KE + PE) is presented in Figure 19e, and a dissipation of energy is observed at the switching times.

6 Conclusions and future perspectives

This paper addresses the modelling and numerical integration of multibody systems whose bilateral constraints abruptly change with respect to switching functions and thus exhibit some nonsmoothness in time. These switching functions define switching surfaces, that punctuate the system dynamics into smooth and nonsmooth dynamical regimes or modes. Different definitions of switching surfaces may result in distinct constraint spaces. Switching surfaces are thus important elements of the model, as they control the geometry of the constraint space.

We present the nonsmooth equations of motion of switched multibody systems in two forms: as hybrid differential-algebraic equations (HDAE), or based on an equality of differential measures. An HDAE comprises two sets of equations: (i) a classical index-3 DAE that holds in the smooth modes, and (ii) an impact equation that defines the impulsive dynamics at switching surfaces. Alternatively, based on the theory of differential measures, a unified set of equations that holds in the smooth modes and at switching surfaces is obtained. These two forms lend themselves to particular choices of time integration schemes.

Regarding the impact law, there is an indeterminacy in the constraint gradient at the switching surface, which affects the expression of the constraint reaction forces. We propose to define the impact law based on an intermediate gradient between the pre- and post-switch gradients. Theoretical arguments and numerical results prove that the choice of this intermediate gradient drives the energy behaviour at switching. Particularly, we show that when it is simply defined as the post-switch gradient, a dissipation of energy occurs. On the contrary, when it is chosen as the bisector of pre- and post-switch gradients, the energy is conserved at switching, at least for systems with a single constraint. For systems with a single constraint, an interpolation formula is presented to parameterize the intermediate gradient using an interpolation parameter. The generalization of such an interpolation to systems with multiple constraints is not trivial but some relevant suggestions were given in the paper.

Next, we perform an analysis and comparison of several possible numerical schemes that could be considered for this class of problems. We choose several versions of the generalized-α method, that include index-3, index-2, and index-1 classical forms, as well as event-driven and time-stepping versions of the generalized-α (NSGA) scheme. In a benchmark test, we observe that the index-3 solution is contaminated with spurious oscillations, while the index-1 solution gives inaccurate results. Using the index-2 and nonsmooth schemes, we further study the energy behaviour at switching. The index-2 solution gives unacceptable results, unless a specific set of coefficients are

selected. The nonsmooth generalized-α method (NSGA) gives accurate results and can handle the nonsmooth dynamics of switching bilateral constraints in a robust and efficient manner.

The NSGA was successfully applied to them simulation of three additional models of mechanical systems with switching bilateral constraints: the model of a braiding machine, which shows the existence of smooth and switched constraints, the model of a wheel rolling across a pothole, which shows the formulation of systems with multiple switching surfaces, and a cam-follower mechanism with a periodic definition of switching surfaces.

7 Acknowledgements

This work was supported by the European Union's Horizon 2020 research and innovation programme under the Marie Skłodowska-Curie grant agreement No. 860124. This publication reflects only the author's view and the Research Executive Agency is not responsible for any use that may be made of the information it contains.

Conflict of interest

The authors declare that they have no conflict of interest.

Data availability

The data supporting the findings of this study are available within the paper.

References

[1] Michel Géradin and Alberto Cardona. *Flexible Multibody Dynamics: A Finite Element Approach*. John Wiley & Sons, Chichester, 2001.

[2] Friedrich Pfeiffer. Multibody systems with unilateral constraints. *Journal of Applied Mathematics and Mechanics*, 65:665–670, 2001.

[3] Bernard Brogliato. Nonsmooth Mechanics: Models, Dynamics and Control. Switzerland, 2016. Springer International Publishing.

[4] Christian Studer. *Numerics of unilateral contacts and friction. Modeling and numerical time integration in non-smooth dynamics*. Springer, Berlin, 2009.

[5] Frédéric Dubois, Vincent Acary, and Michel Jean. The contact dynamics method: A nonsmooth story. *Comptes Rendus Mécanique*, 346(3):247–262, 2018. The legacy of Jean-Jacques Moreau in mechanics / L'héritage de Jean-Jacques Moreau en mécanique.

[6] Michel Jean, Vincent Acary, and Yann Monerie. Non-smooth contact dynamics approach of cohesive materials. *Philosophical Transactions of the Royal Society of London. Series A: Mathematical, Physical and Engineering Sciences*, 359(1789):2497–2518, 2001.

[7] Stephan Trenn. Switched differential algebraic equations. *Dynamics and Control of Switched Electronic Systems: Advanced Perspectives for Modeling, Simulation and Control of Power Converters*, pages 189–216, 2012.

[8] Stephan Trenn. Stability of switched DAEs. *Hybrid Systems with Constraints*, pages 57–83, 2013.

[9] Zhendong Sun and Shuzhi Sam Ge. *Stability theory of switched dynamical systems*. Springer, London, 2011.

[10] Daniel Liberzon and A Stephen Morse. Basic problems in stability and design of switched systems. *IEEE control systems magazine*, 19(5):59–70, 1999.

[11] Jorge Cortes. Discontinuous dynamical systems. *IEEE Control systems magazine*, 28(3):36–73, 2008.

[12] Arjan J van der Schaft and Johannes Maria Schumacher. Complementarity modeling of hybrid systems. *IEEE Transactions on Automatic Control*, 43(4):483–490, 1998.

[13] Daniel Liberzon, Joao P Hespanha, and A Stephen Morse. Stability of switched systems: a Lie-algebraic condition. *Systems & Control Letters*, 37(3):117–122, 1999.

[14] Martin Buss, Markus Glocker, Michael Hardt, Oskar Von Stryk, Roland Bulirsch, and Günther Schmidt. Nonlinear hybrid dynamical systems: modeling, optimal control, and applications. In *Modelling, Analysis, and Design of Hybrid Systems*, pages 311–335. Springer, 2002.

[15] Vadim Utkin. Variable structure systems with sliding modes. *IEEE Transactions on Automatic control*, 22(2):212–222, 1977.

[16] Brian T Baumrucker and Lorenz T Biegler. MPEC strategies for optimization of a class of hybrid dynamic systems. *Journal of Process Control*, 19(8):1248–1256, 2009.

[17] Thomas A Henzinger. The theory of hybrid automata. In *Proceedings 11th Annual IEEE Symposium on Logic in Computer Science*, pages 278–292. IEEE, 1996.

[18] Volker Mehrmann and Lena Wunderlich. Hybrid systems of differential-algebraic equations–analysis and numerical solution. *Journal of Process Control*, 19(8):1218–1228, 2009.

[19] Rafal Goebel, Ricardo G Sanfelice, and Andrew R Teel. Hybrid dynamical systems. *IEEE control systems magazine*, 29(2):28–93, 2009.

[20] Albert Benveniste, Benoît Caillaud, Hilding Elmqvist, Khalil Ghorbal, Martin Otter, and Marc Pouzet. Structural analysis of multi-mode DAE systems. In *Proceedings of the 20th International Conference on Hybrid Systems: Computation and Control*, pages 253–263, 2017.

[21] S Leela. Stability of measure differential equations. *Pacific Journal of Mathematics*, 55(2):489–498, 1974.

[22] Bernard Brogliato. Impulsive dynamics and measure differential equations. *Nonsmooth Mechanics: Models, Dynamics and Control*, pages 1–49, 2016.

[23] Vincent Acary, Olivier Bonnefon, and Bernard Brogliato. Time-stepping numerical simulation of switched circuits within the nonsmooth dynamical systems approach. *IEEE Transactions on Computer-Aided Design of Integrated Circuits and Systems*, 29(7):1042–1055, 2010.

[24] Alexandre Rocca, Vincent Acary, and Bernard Brogliato. Index-2 hybrid DAE: a case study with well-posedness and numerical analysis. *IFAC-PapersOnLine*, 53(2):1888–1893, 2020.

[25] Vincent Acary and Bernard Brogliato. *Numerical Methods for Nonsmooth Dynamical Systems: Applications in Mechanics and Electronics*, volume 35. Springer, Berlin, 2008.

[26] Mounia Haddouni, Vincent Acary, Stéphane Garreau, Jean-Daniel Beley, and Bernard Brogliato. Comparison of several formulations and integration methods for the resolution of DAEs formulations in event-driven simulation of nonsmooth frictionless multibody dynamics. *Multibody System Dynamics*, 41(3):201–231, 2017.

[27] Vincent Acary. Projected event-capturing time-stepping schemes for nonsmooth mechanical systems with unilateral contact and Coulomb's friction. *Computer Methods in Applied Mechanics and Engineering*, 256:224–250, 2013.

[28] Alejandro Cosimo, Javier Galvez, Federico J Cavalieri, Alberto Cardona, and Olivier Brüls. A robust nonsmooth generalized-α scheme for flexible systems with impacts. *Multibody System Dynamics*, 48(2):127–149, 2020.

[29] Olivier Brüls, Vincent Acary, and Alberto Cardona. Simultaneous enforcement of constraints at position and velocity levels in the nonsmooth generalized-α scheme. *Computer Methods in Applied Mechanics and Engineering*, 281:131–161, 2014.

[30] Armin Nurkanović, Jonathan Frey, Anton Pozharskiy, and Moritz Diehl. Finite elements with switch detection for direct optimal control of nonsmooth systems with set-valued step functions. In *2023 62nd IEEE Conference on Decision and Control (CDC)*, pages 5286–5293, 2023.

[31] Vincent Acary, Hidde De Jong, and Bernard Brogliato. Numerical simulation of piecewise-linear models of gene regulatory networks using complementarity systems. *Physica D: Nonlinear Phenomena*, 269:103–119, 2014.

[32] Yung-Chow Wong. Differential geometry of Grassmann manifolds. *Proceedings of the National Academy of Sciences*, 57(3):589–594, 1967.

[33] Konstantin Usevich and Ivan Markovsky. Optimization on a Grassmann manifold with application to system identification. *Automatica*, 50(6):1656–1662, 2014.

[34] David Amsallem and Charbel Farhat. Interpolation method for adapting reduced-order models and application to aeroelasticity. *AIAA journal*, 46(7):1803–1813, 2008.

[35] P-A Absil, Robert Mahony, and Rodolphe Sepulchre. Riemannian geometry of Grassmann manifolds with a view on algorithmic computation. *Acta Applicandae Mathematica*, 80:199–220, 2004.

[36] Martin Arnold and Olivier Brüls. Convergence of the generalized-α scheme for constrained mechanical systems. *Multibody System Dynamics*, 18:185–202, 2007.

[37] Charles William Gear, Ben Leimkuhler, and Gopal K Gupta. Automatic integration of Euler-Lagrange equations with constraints. *Journal of Computational and Applied Mathematics*, 12:77–90, 1985.